Fatigue and Fracture of Pyrolytic Carbon: A Damage-Tolerant Approach to Structural Integrity and Life Prediction in "Ceramic" Heart Valve Prostheses

Robert O. Ritchie

Department of Materials Science and Mineral Engineering, University of California, California, USA

Background and aims of the study: **The fracture and fatigue properties of Si-alloyed LTI pyrolytic carbon and pyrolytic carbon-coated graphite are described as a framework for establishing damage-tolerant analyses for maintaining structural integrity and for predicting the lifetimes of mechanical heart valve prostheses fabricated from these materials.**
Methods: **The analyses are based on fracture-mechanics concepts and provide conservative (worst-case) estimates of the time, or number of loading cycles, before the valve will fail, or more precisely for pre-existing defects in valve components to grow subcritically to critical size under elevated physiologic loading and environmental conditions.**
Results: **For structural life in excess of patient lifetimes, a minimum required detectable defect size is computed which must be detected by quality-control procedures prior to the device entering service; this defect size is typically of the order of tens of microns for such "ceramic" valves, compared to sizes in the hundreds of microns for corresponding metal valves.**
Conclusions: **It is concluded that in light of the brittle nature of pyrolytic carbon and the unacceptable cost of mechanical valve failures, the use of such analyses should be regarded as essential in order to provide maximum assurance of patient safety.**

The Journal of Heart Valve Disease 1996;5(Suppl. I): S9 - S31

Mechanical heart valve prostheses are designed to regulate blood flow continuously in hostile physiologic environments for periods in excess of patient lifetimes. Valve components are exposed to cyclic loading, flexing and bending, wear at surfaces exposed to articulation, and cavitation erosion on surfaces exposed to blood flow. Silicon-alloyed low-temperature isotropic (LTI) pyrolytic carbon has been shown to be a successful material for this application (1-4), has been used in over 600,000 implanted valves and is currently used in the majority of artificial heart valves that are commercially available (5).

Most modern heart valves are generally constructed with two semi-circular leaflets (bileaflets), or with a tilting disc (occluder), which open(s) and close(s) as the heart beats, thereby regulating blood flow under near-normal rheological conditions. The leaflets or disc are contained in a circular housing (or orifice), which in certain valves is stiffened by a metallic restraining ring; a cloth sewing ring is affixed to the outer diameter to facilitate attachment to cardiac tissue.

In the U.S., the disc or leaflets are invariably manufactured from pyrolytic carbon-coated graphite; the housing can also be manufactured from this material, or alternatively from pure pyrolytic carbon, titanium or cobalt-chromium alloys. Unfortunately, the complex shapes of some of the metallic components have required the use of casting and welding technologies in their fabrication. As a result, serious structural problems have arisen with certain of these devices, leading to many implant failures due to fatigue cracking in the valve housing (6-9). Accordingly, the majority of heart valves implanted in the U.S. today are made entirely from ceramic-like material, i.e., from pyrolytic carbon and/or a pyrolytic carbon/graphite laminate. Examples of such valves are shown in Figure 1.

One of the primary restrictions on artificial heart valves is their potentially uncertain lifetime under complex physiologic loading due to degradation by cyclic fatigue or stress corrosion. While hundreds of thousands of pyrocarbon heart valves have been successfully implanted, over forty recent structural failures, involving principally leaflet fractures, have been reported and in many cases attributed to cyclic fatigue (10). An example of such an in vivo leaflet failure is shown in Figure 2. In this instance, cracking was possibly initiated by cyclic fatigue prior to catastrophic overload fracture. Although the latter conclusion may be somewhat questionable due to the difficulty in distinguishing fractographic features produced under cyclic

Address for correspondence:
Robert O. Ritchie, Department of Materials Science and Mineral Engineering, University of California, Berkeley, CA 94720-1760, USA

Figure 1: A selection of commercial pyrolytic-carbon bileaflet and tilting-disc prosthetic heart valves. A metallic tilting-disc valve (with a Co-Cr alloy housing and a pyrolytic carbon/graphite occluder) is shown for comparison (bottom left).

versus impact loading conditions (11), these failures do serve to illustrate that careful mechanical design and accurate life prediction are essential elements for the safe, reliable operation of heart valve prostheses, which must endure sustained physiologic loading and environmentally induced degradation throughout their service lifetime.

Since the human heart beats some 40 million times per year, the primary mechanism of structural degradation can be considered to be cyclic fatigue. Accordingly, to maintain structural integrity, prosthetic heart valves must be designed to endure fatigue lifetimes in excess of 10^9 cycles in physiologic environments. To achieve this, fatigue-life estimation procedures have been developed (12), initially for metal (12) and subsequently for pyrocarbon (13) valves, based on both stress/life and so-called damage-tolerant approaches; currently, however, because of the safety-critical nature of replacement heart valve applications, Food and Drug Administration (FDA) requirements (14,15) demand that for mechanical valves, damage-tolerant design analyses are used.

The latter approach relies on the fracture-mechanics based concept that a conservative (worst case) estimate of the structural life can be defined in terms of the time, or number of loading cycles, for the largest undetected crack to grow to critical size, generally defined as the onset of catastrophic failure of the component in terms of the material's fracture toughness, K_c. A similar analysis might be required for other forms of subcritical crack growth, for example, by stress-corrosion cracking (static fatigue) in components subject to sustained (non-cyclic) loads.

In this paper, damage-tolerant design and life-prediction procedures are described for mechanical heart-valve prostheses, with specific reference to cardiac devices manufactured from ceramic-like pyrocarbon materials. The analyses are performed on a hypothetical bileaflet valve and serve to determine the safe implant life as a function of the size and nature of pre-existing defects in the valve material. Based on such calculations, a minimum required detectable crack size (12) is computed, which must be discovered by quality control procedures prior to the device entering service to ensure safe operation of the valve. It is shown that this minimum crack size can be of the order of tens of microns for pyrocarbon valves, compared to sizes in the hundreds of microns for the metal valves.

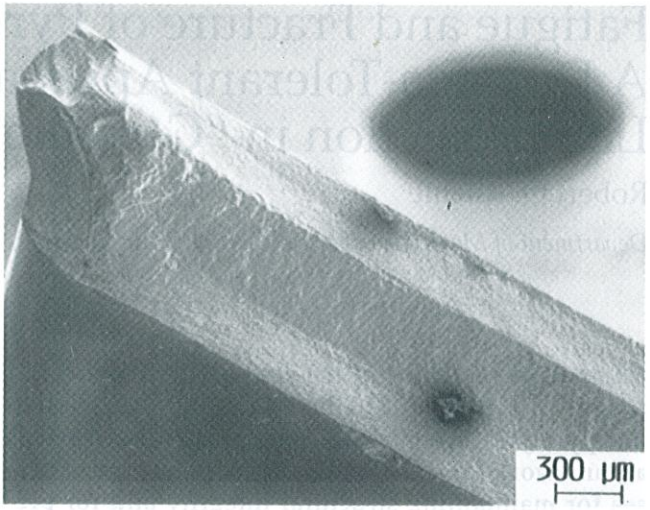

Figure 2: Example of an in vivo failure in a pyrolytic-carbon coated graphite leaflet, where cracking was possibly initiated in cyclic fatigue prior to final overload fracture.

Pyrolytic carbon materials

Structure and processing

Three types of carbon are commonly used for biomedical devices; the low-temperature isotropic (LTI) form of pyrolytic carbon, glassy (vitreous) carbon, and the ultra low-temperature isotropic (ULTI) form of vapor-deposited carbon; all have a disordered lattice structure and are collectively referred to as turbostratic carbons (1,2,4). Although pyrolytic carbons were originally developed for elevated-temperature applications (e.g., coatings for nuclear fuel particles), LTI pyrolytic carbon has found greatest appeal in the biomaterials industry for mechanical cardiac valve components as it has been shown to be highly thromboresistant and to have inherent cellular biocompatibility with blood and soft tissue (4); moreover, it displays good durability, strength and resistance to wear (16,17), and had been thought to be immune to cyclic fatigue failure (18,19).

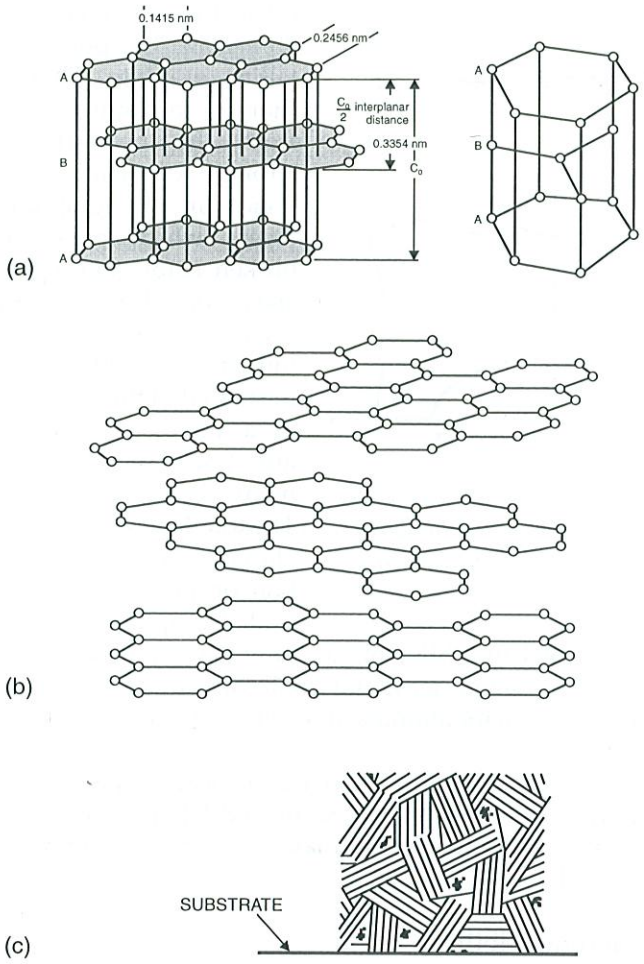

Figure 3: The crystallographic arrangement of carbon atoms in (a) hexagonal graphite where parallel layer planes are in a regular sequence, and (b) a turbostratic carbon where the layers are arranged without order. Randomly oriented turbostratic crystallites are assembled to produce a bulk material in (c). Adapted from reference 3.

The structure of turbostratic carbons is closely related to that of graphite (Fig. 3a). In a single crystal of graphite, the carbon atoms are covalently bonded in planar hexagonal arrays which are stacked in layers in a regular ABAB sequence with relatively weak van der Waals interlayer bonding; in polycrystalline graphite, these crystals, or "crystallites", typically have diameters larger than 100 nm. With turbostratic carbons, the stacking sequence is disordered through random rotations or displacements of the layers relative to each other (Fig. 3b); moreover, wrinkles or distortions may exist within each layer from imperfect matching of small layer segments due to missing carbon atoms. This structural distortion has a marked effect on density, which can vary from 1,400 $kg.m^{-3}$ to a theoretical limiting value of 2,200 $kg.m^{-3}$. Crystallites in turbostratic carbon are much smaller (≈10 nm) than in graphite, and are randomly oriented to produce the bulk material (Fig. 3c) (20); thus, on a macroscale which is large compared to the crystallite size, the material behaves in an isotropic fashion.

For heart valve devices, a silicon-alloyed LTI-pyrolytic carbon is used, either as a ≈250-μm thick coating on a polycrystalline graphite substrate or as a monolithic material where the substrate is machined away; 10 to 20 wt% silicon is added to improve mechanical properties, i.e., stiffness, hardness, wear resistance, without significant loss in biocompatibility. Components are typically made by co-depositing carbon and silicon carbide on the graphite substrate via a chemical vapor-deposition, fluidized-bed process using a gaseous mixture of a Si-containing carrier gas with a hydrocarbon (e.g., propane, methyltrichlorosilane and helium gas mixtures); the pyrolysis occurs at temperatures of 1000°C to 1500°C (21). The resulting pyrocarbon contains typically 10 wt% silicon, often in the form of discrete sub-micron β-SiC particles, randomly dispersed in a matrix of roughly spherical micron-size "growth features" (subgrains) of subcrystalline turbostratic carbon, containing ≈10 nm sized crystallites (22,23).

Residual stress

Biomedical turbostratic carbon coatings often exist in a state of residual stress. Like most coatings cooled from a higher processing temperature, the residual stress state depends on the difference in thermal expansion mismatch between the coating and the underlying substrate material. In addition, variation in the structure and grain size of the coating from the interface with the substrate to the coating surface may also affect the residual stress state. Both these effects are also dependent on the coating thickness. For LTI pyrolytic carbon-coated graphite components, the greater thermal expansion coefficient of pyrolytic carbon compared to graphite results in a tensile residual stress in the coating. Depending on processing temperature and microstructural variation, various measurements seem to indicate a tensile stress of up to 60 MPa, which is often at a maximum near the surface of the coating and approaches zero at the pyrolytic carbon/graphite interface (13). Such residual stresses may be particularly detrimental to the integrity of the coating as their value must be added to the nominal applied stress when evaluating the likelihood of fracture in the coating.

Mechanical properties

The mechanical properties of turbostratic carbons are closely related to their coating density as the extent of porosity affects the internal area over which stress is distributed; properties also depend on specific composition and microstructure, including the volume fraction of SiC particles and the size of the crystallites and

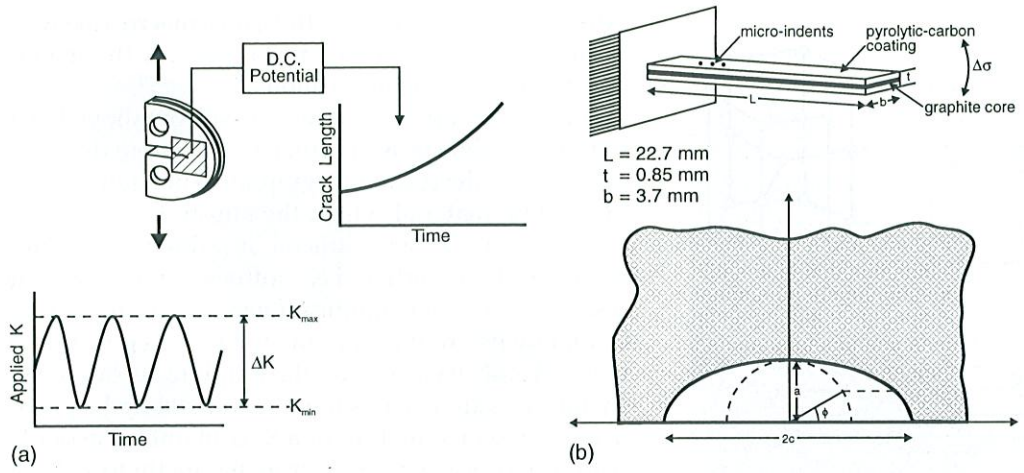

Figure 4: Experimental techniques used to measure cyclic fatigue-crack propagation rates, showing (a) half round compact (leaflet) specimen and procedures used to monitor crack length for long through-thickness (edge) cracks, and (b) cantilever-bend specimen (with micro-indents) showing semi-elliptical surface crack configuration for tests on small cracks (26).

"growth features" (2,16,17,24). Unlike certain forms of carbon with a high degree of preferred orientation and high density which are extremely strong and stiff in directions parallel to the preferred layer planes, because crystallites are randomly arranged and the material is not fully dense, LTI pyrolytic carbon has an uncharacteristically low modulus and comparatively high strength. Values of Young's modulus are typically between 27 and 31 GPa, which is close to the upper bound value for bone of 21 GPa and an order of magnitude less than that of surgical stainless steel or titanium alloys. The hardness, and hence wear resistance, of pyrolytic carbons is also a function of crystallite size and SiC content; in fact, Si-alloyed pyrolytic carbon has superior wear resistance to either graphite or unalloyed pyrolytic carbon (2).

The high strength and low moduli of turbostratic carbons results in large strains to failure when compared to other brittle ceramics, i.e., LTI pyrolytic carbon has a fracture strain of 1.5%- 2.0%, compared to ≥ 0.1% for alumina and 0.1%-0.7% for polycrystalline graphite. This is thought to result in part from the network of strong covalent C-C bonds in the graphitic layers which must be broken before failure by shear or cleavage can occur. However, fracture toughness values, K_c, measured in the presence of a pre-existing crack, are low compared to many ceramics (5,25,26). The toughness of pure Si-alloyed LTI pyrolytic carbon or pyrolytic carbon coated graphite is of the order of 1 to 2 MPa√m, i.e., only slightly higher than that of soda lime glass and small compared to a K_c of ≈3 to 6 MPa√m for alumina and ≈3 to 15 MPa√m for zirconia (5).

A list of structural and mechanical properties for polycrystalline graphite, Si-alloyed LTI pyrolytic carbon and pyrolytic-carbon coated graphite is given in Table I.

Biocompatibility

High-purity turbostratic carbons, like LTI pyrolytic carbon, have exceptionally good cellular biocompatibility and thromboresistance (2). For cardiovascular applications, compatibility with blood has received the most attention; unlike soft and hard tissue reactions to implanted materials which develop slowly, the rejective reactions in blood are dramatic and swift. Most materials in contact with blood quickly activate the tissue's clotting mechanism; LTI carbon has been shown to be equivalent to siliconized glass, which causes little

Table I: Structural and mechanical properties of graphite, Si-Alloyed LTI pyrolytic carbon, and graphite/pyrolytic carbon laminate (5)

Property	Polycrystalline Graphite Substrate	Si-Alloyed LTI Pyrolytic Carbon	Si-Alloyed LTI Pyrolytic-Carbon Coated Graphite
Density (kg.m^{-3}	1500-1800	1700-2200	1500-2200
Crystallite Size (nm)	15-250	3-5	-
Expansion Coefficient (10^{-6} K^{-1})	0.5-5	5-6	2-6
Hardness (DPH)	50-120	230-370	232-412
Young's Modulus (GPa)	4-12	27-31	34.5
Flexural Strength (MPa)	65-300	350-530	-
Fracture Strain (%)	0.1-0.7	1.5-2.0	1.5-2.0
Fracture Toughness, K_c (MPa√m)	~1.5	0.9-1.1	1.0-2.6

damage to blood. Theories to explain the excellent cellular biocompatibitily of LTI carbon with blood range from conditioning of the carbon surface with a passivating protein layer through selective adsorption to the complete inertness of the LTI carbon surface to proteins in general. A general observation, however, is that smooth or polished surfaces are better than rough surfaces, possibly because roughness may provide locations where cells can adhere and serve as thrombotic nuclei.

Fatigue and fracture mechanics

The prediction of a safe lifetime is clearly a vital step in the design and operation of any structural component. In situations where stresses are primarily alternating, as in the case of heart valve prostheses, there are two approaches that can be used, namely the classical stress/life (S/N) approach and the damage- (or defect) tolerant approach which is based on fracture mechanics (12). With S/N analyses, smooth-sided or notched test specimens are cycled to failure at specific values of the stress or strain (defined as both a range and a mean) with the objective of relating the total life (i.e., the number of cycles both to initiate and propagate a crack to failure) to the stress or strain (27).

Lifetime predictions are made based on such S/N data, often following adjustments for such variables as notch geometry, variable-amplitude loading, environment, frequency, and so forth. Although used for numerous engineering situations, such as in the design of small components such as gears, the approach is not favored for safety-critical situations, such as prosthetic heart valves, where loss of life is a possibility. This is because lifetimes are computed from laboratory-derived data representing the time or cycles both to initiate and propagate a crack; since actual components often contain significant pre-existing cracks, there is always a potential for non-conservative lifetime prediction with the S/N approach.

Accordingly, where the cost (either social or financial) of a failure is too high, the alternative damage-tolerant approach must be adopted. This approach essentially assumes that all components already contain pre-existing defects and life is determined in terms of how long it takes these defects to extend to failure; such an approach has become mandatory for many nuclear and aerospace applications. Specifically, the concept of damage-tolerant design relies on the notion that the minimum safe structural life of a component can be determined from the time, or number of loading cycles, for incipient cracks to grow subcritically to instability or until catastrophic failure occurs.

For a "ceramic" heart valve prosthesis subjected to roughly 40 million cycles a year, this translates into the time for the largest pre-existing defect to grow by cyclic fatigue (and/or stress corrosion) until final fracture ensues at K_c (12). Accordingly, to estimate this life, a characterization of subcritical crack-growth rates for laboratory samples or actual components tested under realistic service (i.e., in vitro) conditions must be determined, and then integrated between the limits of the initial and final crack sizes. Such characterization can be achieved using fracture mechanics, the principles of which are described below.

Fracture mechanics

Concepts

For small scale yielding conditions where the overall deformation in the component is nominally linear elastic and only limited inelasticity (e.g., plasticity) is present, the "driving force" for crack extension can be defined in terms of a stress intensity K which uniquely and autonomously characterizes the distribution of local stresses and displacements in the vicinity of the crack tip, viz:

$$K = Q\sigma_{app}\sqrt{\pi a}, \qquad (1)$$

where a is the crack length, σ_{app} is the applied stress (which can include both externally applied stresses and residual stresses), and Q is a geometry factor (which is generally a function of a) of order unity. Since K characterizes the local crack-tip field, its value can therefore be correlated to the extent of crack extension.

Such concepts can be readily used to quantify the toughness of the material, specifically in terms of the critical value of the stress intensity at the onset of unstable (i.e., catastrophic) fracture. Provided conditions of small scale yielding and plane strain exist, this critical value of stress intensity is referred to as the fracture toughness, K_c, and is considered to be a material constant. Conditions of small scale yielding and plane strain are relevant provided the extent of the local inelasticity, e.g. the crack-tip plastic-zone size, is small compared to the in-plane (e.g. crack length a) and out-of-plane (e.g. test-piece thickness B) specimen directions, respectively.

According to ASTM standards (28), this can be achieved when $a,B \geq 2.5\,(K/\sigma_y)^2$, where σ_y is the yield or flow stress of the material. The fracture toughness can be used to define another important concept, that of the critical crack size, a_c, which represents the largest crack that can be tolerated by the component without catastrophic failure. Since failure occurs at $K = K_c$, the critical crack size, for a particular applied stress, can be determined simply from the relevant K solution, e.g., from Equation 1:

$$a_c = \frac{1}{\pi}\left(\frac{K_c}{Q\sigma_{app}}\right)^2. \qquad (2)$$

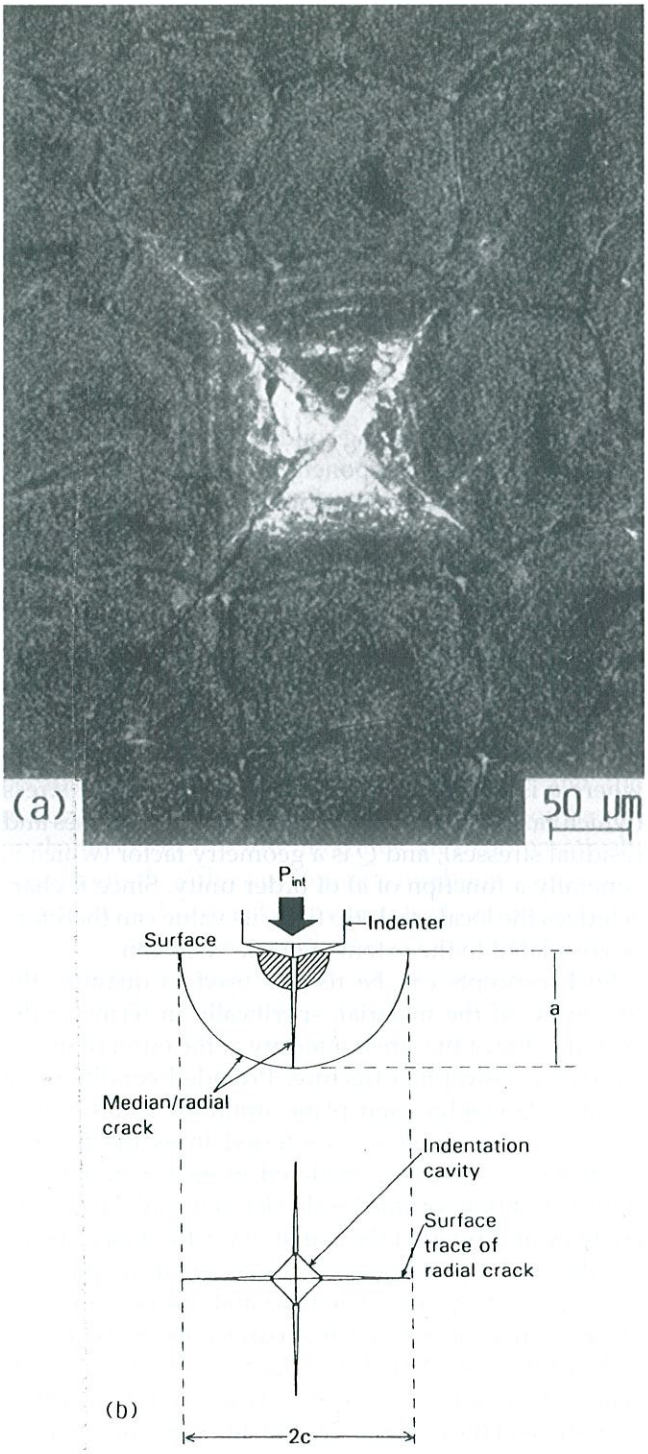

Figure 5: (a) Optical micrograph of a Vicker's indent (indentation load P_{int} = 10 kg) on pyrolytic-carbon coating, showing median/radial cracks emanating from the indent; (b) schematic illustration of the indentation system and crack configuration showing the characteristic crack-size dimensions a and c (37).

Measurement

Several standards are available for the measurement of fracture toughness values; ASTM Standard E-399 (28) is perhaps the most important, although similar to corresponding European and Japanese standards, it was developed primarily for metallic materials under solely linear-elastic conditions. Where more than limited inelasticity is present, or where extensive slow crack growth precedes unstable fracture, alternative standards for, respectively, non-linear elastic fracture mechanics (e.g. ASTM E-813) and, resistance-curve behavior (e.g. ASTM E-561) can be used (28).

In simple terms, fracture toughness K_c values are ideally measured on compact-tension or single-edge-notched bend samples (Fig. 4a), which have been pre-cracked (typically by cyclic fatigue) prior to testing; specimens are loaded monotonically to instability, and the critical value of K computed from the load, P, and crack length, a, at failure. For most standard specimen geometries, handbook K solutions are used (29), e.g., for the compact-tension C(T) specimen:

$$K = \left(\frac{P}{BW^{1/2}}\right) f\left(\frac{a}{W}\right), \tag{3}$$

where B and W are respectively the test piece thickness and width, and $f(a/W)$ is a function of a/W tabulated in references #28 and #29. Although the toughness is generally defined under linear-elastic conditions at the onset of unstable fracture, in many toughened ceramics and in metals where extensive plasticity accompanies fracture, slow (stable) crack extension, Δa, can occur under increasing stress-intensity levels prior to instability; such behavior is termed a resistance (or R-) curve, and can be used to define the toughness, either at crack initiation (where $\Delta a \rightarrow 0$) or further out on the R-curve under nominal steady-state conditions (30).

Since it is generally difficult to fatigue pre-crack many brittle materials, the fracture toughness of ceramics can be approximated using indentation techniques (31,32). Specifically, the K_c value can be estimated from the size of the radial cracks emanating from Vicker's hardness indents at high applied indentation loads (Fig. 5); for pyrolytic carbon, this load is typically in excess of 9 kg. The radial cracking forms in response to the residual tensile stress field which surrounds the indent on unloading; the stress-intensity factor, K_R, from this field can be computed in terms of the peak indentation load P_{int}, and the half surface-crack length c, by (33):

$$K_R = \chi_R P_{int} c^{-3/2} \tag{4}$$

where χ_R is a material constant dependent upon the ratio of Young's modulus E, to hardness H_v, given by (34):

$$\chi_R = \xi_V (E/H_V)^{1/2}, \tag{5}$$

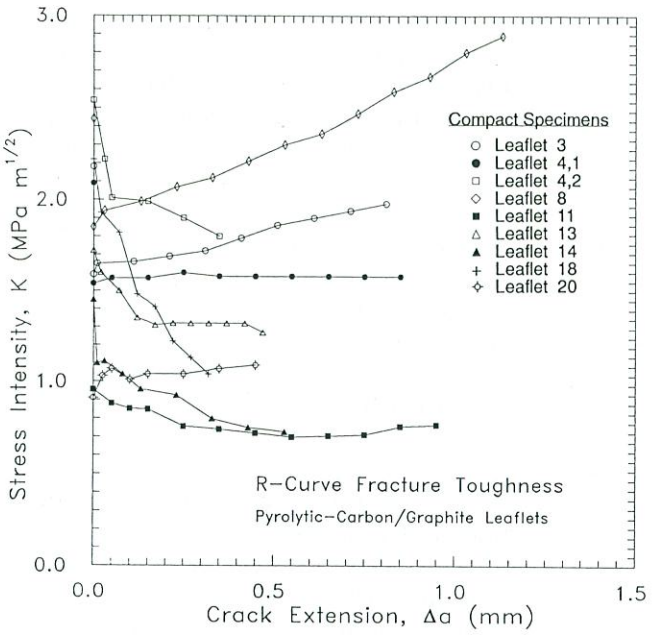

Figure 6: Resistance curves for half-round compact (leaflet) specimens of pyrolytic-carbon coated graphite containing "long" through-thickness (edge) cracks, tested in 37°C Ringer's solution. The fracture toughness, K_c, can be defined either at crack initiation, i.e., as $\Delta a \rightarrow 0$, or at nominal "steady state" on the plateau of the R-curve, if one exists (37).

where ξ_v is a material-independent constant for Vicker's-produced radial cracks with a value of 0.016 (32). The toughness is then simply computed from Equations 4 and 5 at $K_c = K_R$ by denoting c_0 as the equilibrium surface length of the post-indentation crack (31,32). An example of such radial cracking surrounding a Vicker's indent in pyrolytic carbon is shown in Figure 5. Indentation toughness values must be considered to be approximate as they take no account of R-curve behavior; in essence, they are defined for crack arrest at some arbitrary point on the R-curve.

It should be noted that both the ASTM and indentation techniques, described above for measuring fracture toughness values, utilize sharp (i.e., fatigue) precracks as their initial stress concentrator. However, certain authors in past have used notched samples to measure the toughness of brittle materials; since the toughness is known to be a strong function of the root radius of the stress concentrator (35); this can lead to unrealistically high K_c values, as first pointed out for pyrolytic carbon by this author (25). For example, More et al. (36) used machined-notched double-torsion specimens to measure the toughness of pyrolytic carbon and obtained a value of 2.79 ± 0.23 MPa√m, some 50% higher than the accepted K_c value measured with both indentation (26,37) and pre-cracked (25,37-39) samples.

Toughness of pyrolytic carbon

The first fracture toughness measurements on the Si-alloyed LTI pyrolytic carbon-coated graphite material (for the remainder of this paper, the term "pyrolytic carbon" will imply the Si-alloyed low temperature isotropic material that is currently used in the manufacture of heart valve prostheses) using appropriate pre-cracked compact-tension samples yielded K_c values between 1.1 and 1.6 MPa√m for tests in room air and 37°C Ringer's solution (25). The latter solution is used here as a simulated physiologic (blood analog) environment and is prepared by dissolving 8.5 g NaCl, 250 mg KCl and 300 mg $CaCl_2$ in 1000 ml of distilled water. (There is no difference between results in air and Ringer's solution as little effect of the environment would be expected during the brief duration of these tests).

Subsequent studies (13,26,37-39) on both pure (monolithic) pyrolytic carbon and the pyrolytic carbon/graphite laminate generally show complex R-curve behavior with initiation and steady-state toughness values varying between 1 and 2 MPa√m. Within this range, results for pure pyrolytic carbon are invariably at the low end of this range (38,39); for the laminate, the toughness appears to be increased as the ratio of the thickness of the pyrolytic carbon to graphite layers is made smaller (39). It is interesting to note that with thickness ratios below about 2, the toughness of the composite can be higher than either the pyrolytic carbon or graphite layers. Although not completely

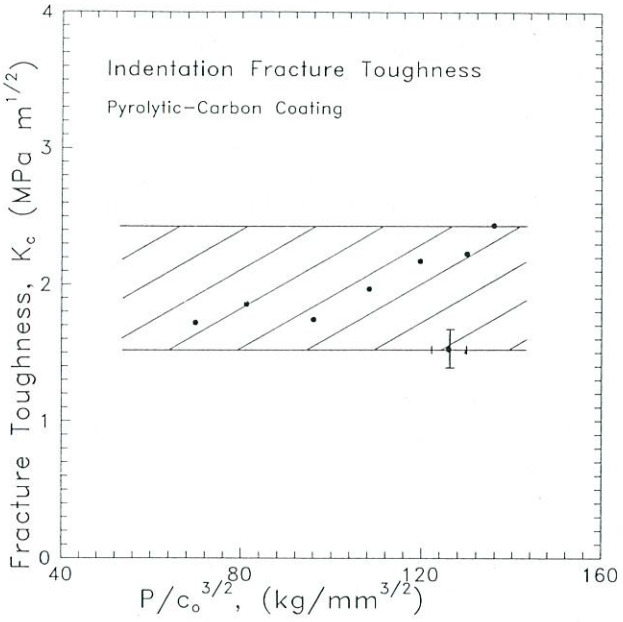

Figure 7: Variation in fracture toughness, K_c, in the presence of "small" cracks in the pyrolytic-carbon coating as a function of the indentation load and equilibrium radial crack depth, $P_{int}c_o^{-3/2}$, as measured using indentation-toughness techniques (37).

understood, this has been attributed to variations in the stress intensity across the crack front due to the inhomogeneous (layered) nature of the material, which causes the crack in the pyrolytic carbon-coating to lead slightly the crack in the graphite substrate (39).

An example of fracture-toughness data for pyrolytic-carbon coated graphite is shown in Figure 6; the average K_c value, measured in 37°C Ringer's solution at crack initiation on compact specimens machined from actual heart valve leaflets, is 1.64 MPa$\sqrt{m}$ (± 0.53 MPa$\sqrt{m}$) (37). Although there is considerable scatter inherent in the data, the results are consistent with those measured using indentation techniques (Fig. 7), where an average K_c of 1.84 MPa$\sqrt{m}$ (± 0.18 MPa$\sqrt{m}$) has been reported (37).

Whereas fracture toughness values between 1 and 2 MPa$\sqrt{m}$ are now accepted for monolithic and composite pyrolytic carbon materials, several points are worthy of note from these results.

First, as mentioned above, the K_c values quoted are significantly less than specific results reported in the literature based on tests on machined-notched samples (36).

Second, the quoted average K_c values were defined at crack initiation; for rising R-curves, this value will not be the maximum stress intensity required for crack extension and thus may be expected to be lower than that measured by indentation techniques.

Third, the 'long' cracks in the compact specimens in Figure 6 are through-thickness (so-called edge cracks) and as such provide an evaluation of the toughness of the pyrocarbon/graphite composite; results from the indentation tests (Fig. 7), on the other hand, sample 'small' surface cracks growing principally in the pyrolytic-carbon coating.

Fourth, residual stresses, which are known to exist in the composite as a result of coating deposition and processing (e.g., from the thermal-expansion mismatch between the pyrolytic-carbon coating and the graphite substrate), may be expected to affect differently the driving force for 'small' cracks in the pyrolytic coating, which is in a state of residual tension, and for 'long' cracks which experience a more complex through-thickness variation in residual stress.

Fifth, the exact value of the constant ξ_v in Equations 4 and 5 and its material independence, which may affect the magnitude of K_c (from Equ. 5), has not been adequately established and remains the subject of some controversy in the literature (32). Moreover, the possible relaxation of the residual stresses due to recovery of the pyrolytic carbon may lead to further uncertainties in Equation 4.

Finally, recent finite-element calculations (39), which take into account the composite elastic-property mismatch between the graphite and pyrolytic-carbon layers, indicate some degree of uncertainty in the stress-intensity solutions for the pyrocarbon/graphite laminate material. Although no studies to date have taken account of this effect, the numerical calculations do show that the K-solutions for homogeneous material (Equ. 3) may underestimate K in the pyrolytic carbon by up to 40% and overestimate K in the graphite layer by up to 60%. However, as shown below, comparisons of the fatigue-crack growth properties in the monolithic pyrolytic carbon and the pyrolytic carbon/graphite laminate, which are characterized in terms of K, do not show such major differences (25,37-39).

Subcritical crack growth

Concepts

Although unstable fracture occurs at the fracture toughness value (under plane-strain conditions where $K = K_c$), subcritical crack growth can occur at lower K levels by mechanisms such as cyclic fatigue and stress-corrosion cracking (static fatigue) (40); in ceramic materials, this typically occurs at stress intensities above ≈50% of K_c (41). Under cyclic loading conditions, the rate of crack growth per cycle, da/dN, can generally be described in terms of power-law relationships, which in their simplest form, can be written as:

$$\frac{da}{dN} = C\Delta K^m, \tag{6a}$$

or

$$\frac{da}{dN} = C'(K_{max})^s(\Delta K)^p, \tag{6b}$$

where ΔK is the applied stress-intensity range, given by the difference in the maximum and minimum stress-intensity values in the cycle, i.e., $\Delta K = K_{max} - K_{min}$, C and C' ($= C(1 - R)^s$) are experimentally-determined scaling constants, and $m = (s + p)$ are the crack-growth exponents. Typically, the exponent m takes values in metals between 2 and 4 (with $p > s$), whereas in ceramic materials, m values can be as high as 100 or more (with $p << s$) (41,42). Similarly, under sustained loading, the corresponding relationships for stress-corrosion crack velocities, da/dt, are of the form:

$$\frac{da}{dt} = C''(K)^n, \tag{7}$$

where C'' and n are scaling constants; values of n are similar to m, i.e., low in metals and high in ceramics. At very low stress intensities, cracks (of a size larger than the dimensions of the microstructure or scale of local inelasticity) may appear to be dormant; these stress intensities are referred to as the fatigue and stress-cor-

rosion thresholds, ΔK_{TH} and K_{TH}, respectively. The cyclic fatigue threshold, ΔK_{TH}, however, is a marked function of the value of the mean (in addition to the alternating) stress, which is generally varied in terms of the so-called load ratio, $R = K_{min}/K_{max}$ (43).

Measurement

Traditional cyclic fatigue-crack growth rates are generally determined using identical specimen geometries to that used for fracture toughness measurement; this involves monitoring the growth of through-thickness (edge) cracks, termed 'long' cracks where lengths exceed several millimeters, in samples such as the compact-tension specimen (Fig. 8a). Material used for these specimens should accurately reflect the material used in the prostheses, i.e., be of clinical grade. Test specimens are typically pre-cracked and cycled, under load, displacement or stress-intensity control, on servo-hydraulic testing machines in appropriate environments, e.g., in simulated physiologic environments such as 37°C Ringer's solution for heart valve materials, and the rate of crack growth computed from measurements of the crack length as a function of the number of cycles (Fig. 8). ASTM standards have been developed for such measurements on metallic materials, specifically E-647 (28); however, as no standards are available for ceramics, the reader is referred to references #25 and #44 for a description of how such tests can be carried out in ceramic-like materials such as pyrolytic carbon.

Although standards also do not exist for stress-corrosion testing, crack velocities are similarly obtained for through-thickness 'long' cracks in appropriate environments on pre-cracked fracture-mechanics type specimen geometries (Fig. 4a), only under sustained (non-cyclic) loads. For brittle materials like pyrolytic carbon, this is best achieved under load-relaxation conditions, i.e., under a constant displacement where the load decreases with increasing crack length. Similar to cyclic fatigue, crack velocity/stress intensity (v/K) plots are derived by continuous monitoring of the crack length at a known load as a function of time.

Cyclic fatigue of pyrolytic carbon

Until fairly recently, it had been assumed that turbostratic carbons such as pyrolytic carbon were insensitive to cyclic fatigue degradation. Early studies (18,19) had claimed that the fatigue endurance strength of these materials was virtually identical to the single-cycle fracture stress, i.e., that cyclic stresses less than this stress do not cause microscopic damage. However, by specifically employing fracture-mechanics type testing procedures with pre-cracked samples, Ritchie et al. (25) first demonstrated unequivocally that fatigue cracks can grow under alternating loads in the pyrolytic-carbon coated graphite laminate in both ambient temperature air and 37°C Ringer's solution.

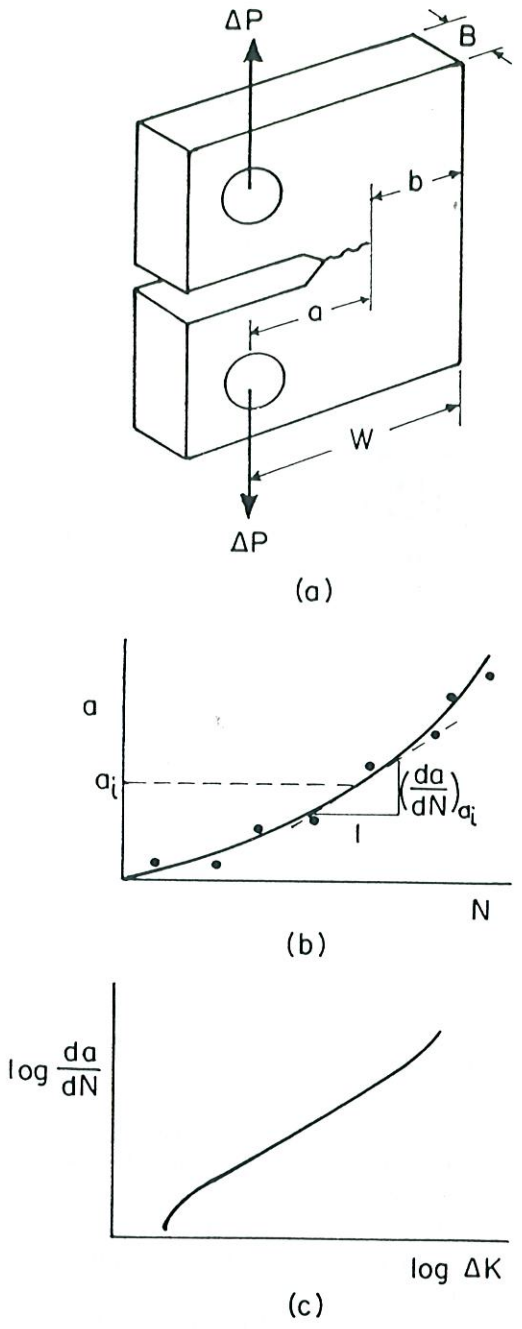

Figure 8: Procedures used for measuring fatigue-crack growth rates, showing compact-tension specimen stressed under cyclic loads, ΔP, b) crack length a versus number of cycles, N, curve differentiated to give growth rate $(da/dN)_{ai}$ at a particular crack length ai, and resulting log-log plot of da/dN versus the stress-intensity range, ΔK.

Subsequent studies have verified that the pyrocarbon/graphite material is indeed susceptible to cyclic fatigue (26,37,39,45), and further shown that fatigue-crack growth can similarly occur in monolithic

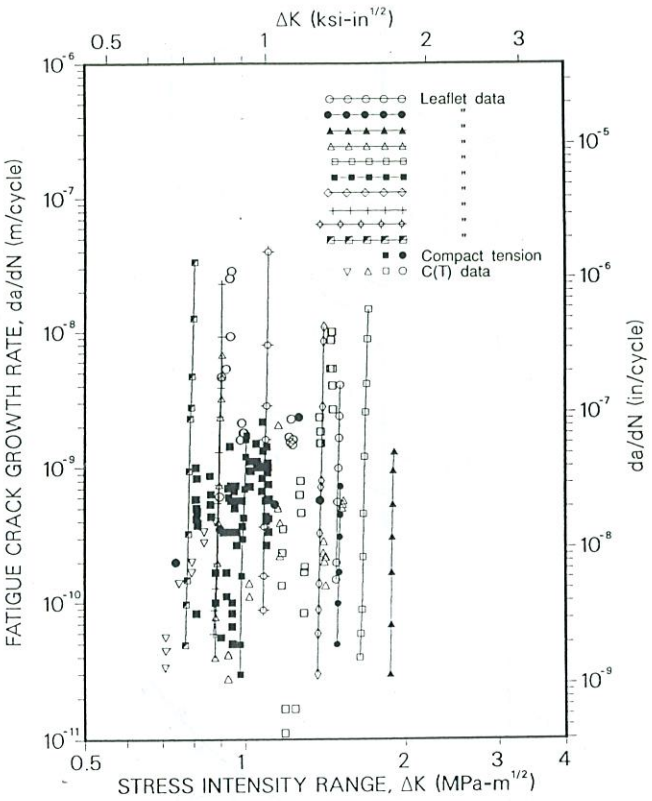

Figure 9: Experimental data showing cyclic fatigue-crack propagation rates, da/dN, as a function of the applied stress-intensity range, ΔK (= 0.9 K_{max}), for half round compact (leaflet) specimens of pyrolytic-carbon coated graphite containing "long" through-thickness (edge) cracks. Results from compact-tension C(T) specimens are included for comparison (25). Tests were performed in a simulated physiological environment of Ringer's solution at 37°C (26).

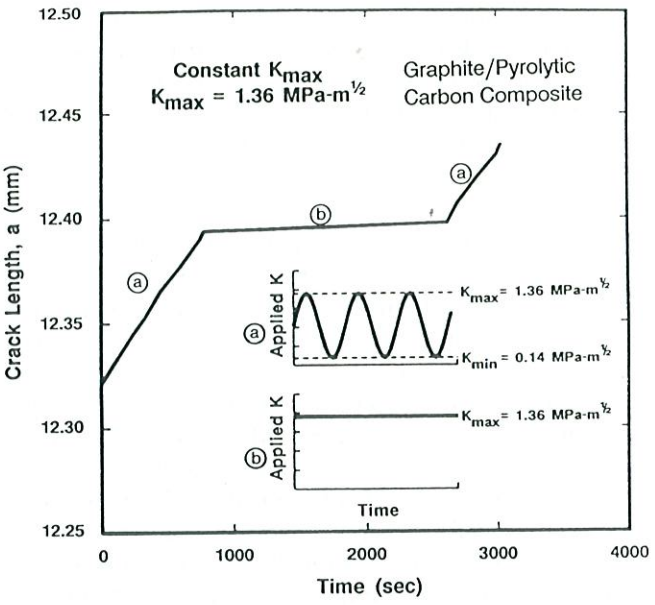

Figure 10: The effect of sustained-load vs. cyclic loading conditions, at a constant K_{max}, on the subcritical crack growth in pyrolytic carbon coated graphite tested in Ringer's solution at 37°C (blood analog). Note how crack-growth rates under cyclic loading (region a) far exceed those measured under sustained loading (region b) (25).

pyrolytic carbon (38,39,46).

Typical crack-growth rate data, for leaflet specimens of the pyrolytic-carbon/graphite laminate tested in 37°C Ringer's solution, are shown in Figure 9 as a function of the stress-intensity range, ΔK (= 0.9 K_{max}). It is apparent that similar to many ceramic materials (41), the slope of these plots, which is characterized by the exponent m in Equation 6, is extremely high; values for pyrolytic carbon materials are routinely well over 100 (37-39). Moreover, similar to R-curve data for pyrolytic carbons (Fig. 6), the growth-rate behavior shows a very high degree of scatter. Based on a comparison of similar fatigue data for ceramic materials tested on the same mechanical-testing machine (41,42), such a wide difference in growth rates (at a given stress intensity) is unusual and appears to result from inherent material differences attributable to variation in fabrication-induced residual stresses or local microstructure. Although measurements on the pyrolytic-carbon coating of leaflets used for manufacturing heart valves do in fact display large variations in residual stress from sample to sample (13), which would indeed affect properties, the precise origin of the scatter in toughness and crack-growth data for this material is still uncertain.

Similar to behavior in many metals and ceramics (41,47), at low growth rates approaching 10^{-11} m/cycle, an apparent fatigue threshold stress-intensity range, ΔK_{TH}, can be defined, below which the growth of 'long' cracks are presumed dormant; in most ceramics, this threshold is of the order of 50% of K_c (41). Based on the results from several studies in 37°C Ringer's solution (13,25,37-39), measured values of ΔK_{TH} for the monolithic and composite pyrolytic carbon materials vary between ≈0.7 and 2 MPa√m, with a typical average value being ≈1 MPa√m. As with toughness data though, within this range, ΔK_{TH} values for pure pyrolytic carbon are at the low end (generally < 1 MPa√m) (38,39), whereas in the laminate, thresholds appear to increase with a decreasing ratio of the thickness of the pyrolytic carbon to graphite layers (39).

While the data in Figure 9 apparently show a clear cyclic effect, in view of past scepticism over cyclic fatigue in turbostratic carbons (18,19), and in fact in ceramic materials in general (48), it has been necessary to demonstrate unequivocally that the crack growth is cyclically induced and not simply a consequence of stress-corrosion cracking at maximum load. To achieve this, crack extension has been monitored with (a) the stress intensity cyclically varied between K_{max} and K_{min},

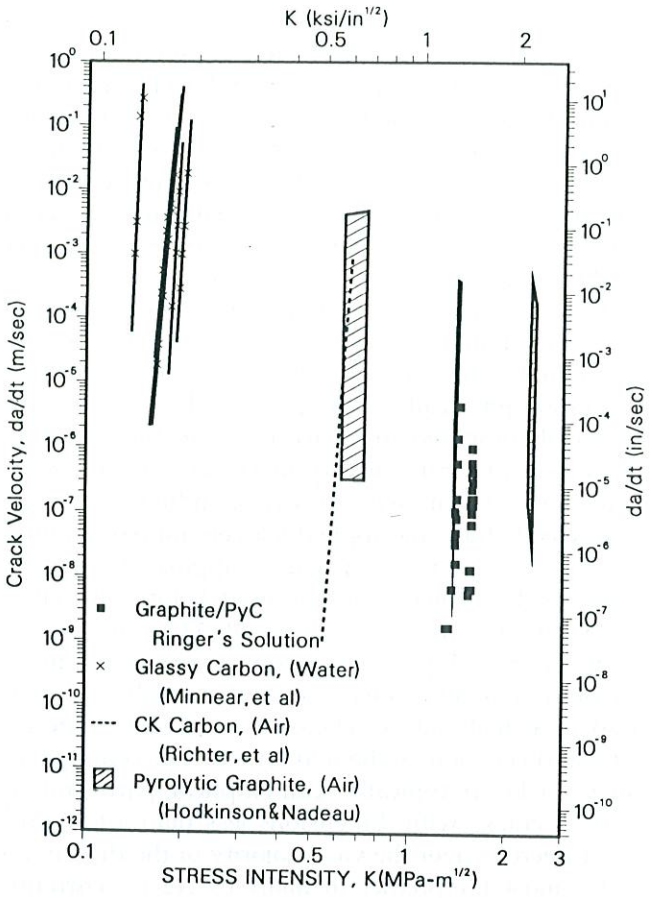

Figure 11: Stress-corrosion crack-growth behavior of LTI pyrolytic-carbon coated graphite composite tested in 37°C Ringer's solution (25), shown in comparison with data for glassy carbon tested in water (49) and air (50) and for pyrolytic graphite in ambient temperature air (51).

and (b) the stress intensity held constant at the same value of K_{max}. A typical result, for K_{max} = 1.36 MPa$\sqrt{m}$ and K_{min} = 0.14 MPa$\sqrt{m}$, is shown in Figure 10 (25).

It is apparent that, whereas crack extension proceeds readily under cyclic loading conditions (region (a)), upon removal of the cyclic component by holding at the same K_{max} (region (b)), crack-growth rates are markedly reduced. Clearly, similar to behavior reported for other ceramic-like materials (41), a true cyclic fatigue effect is apparent; furthermore, subcritical fatigue crack-growth rates under cyclic loading appear to be far in excess of those under equivalent sustained loading. For these reasons, cyclic fatigue must be considered as the dominant mechanism for the extension of cracks in pyrolytic-carbon heart valves; correspondingly, growth-rate data for this mechanism provide the basis for damage-tolerant procedures to predict the safe life of these prostheses.

Stress-corrosion cracking in pyrolytic carbon

Similar to other ceramics, the various forms of carbon are prone to subcritical crack growth under the synergistic action of an applied load and a moist (or corrosive) environment (25,38,49-52). Such stress-corrosion crack-growth behavior is plotted in terms of the crack velocity with respect to time, da/dt, as a function of the applied stress intensity, K, in Figure 11 for several types of carbon (25). The data include a LTI pyrolytic carbon/graphite composite in an environment of Ringer's solution at a temperature of 37°C (25), glassy carbon in water (49) and in air (50), and data for a pyrolytic graphite in air (51). Crack velocities span many orders of magnitude from 10^{-9} to 10^{-1} m/sec and, similar to cyclic fatigue-crack growth, show a marked sensitivity to the stress intensity; values of the exponent n (Equ. 7) typically exceed 100 for pyrolytic carbon (13). Similar to cyclic fatigue, a threshold stress intensity, K_{TH}, can be defined for crack velocities approaching 10^{-10} m/sec; values range between ≈0.8 and 1.8 MPa$\sqrt{m}$, with a typical average value of ≈1.25 MPa$\sqrt{m}$ (13,25). Although crack growth by stress corrosion tends to be slower than by cyclic fatigue (Fig. 10), it is still a viable mechanism for the extension of pre-existing defects in pyrolytic carbons; accordingly, it is important to characterize the stress-corrosion behavior in order to permit the reliable design of a prosthetic device.

Threshold stress intensities

Despite the apparent convenience of a threshold for no apparent crack growth in engineering analysis, which essentially implies that one can design for infinite life, the use of thresholds for either stress corrosion or cyclic fatigue in pyrolytic carbon is not recommended for the design and life prediction in prosthetic heart valves. The primary reason for this is that such devices are expected to endure extremely large lifetimes in excess 10^9 cycles; meaning that subcritical crack growth, if it takes place, may be occurring (at least initially) at vanishingly small growth rates (e.g., below 10^{-12} m/sec), which may be too difficult or time-consuming to measure reliably. Moreover, threshold values may be questionable in view of the small-crack effect, as described below. Accordingly, for conservative lifetime prediction of prosthetic heart valves, it is recommended that, where very low growth-rate data cannot be obtained, a linear extrapolation of higher crack growth vs. K data be used; however, it is imperative for this extrapolation that experimental data are collected at least below growth rates of ≈10^{-10} m/cycle in fatigue and ≈10^{-8} m/sec in stress corrosion.

Small cracks

As described above, most fatigue data for heart valve implants are derived from conventional fracture-mechanics style samples containing 'long' (larger than

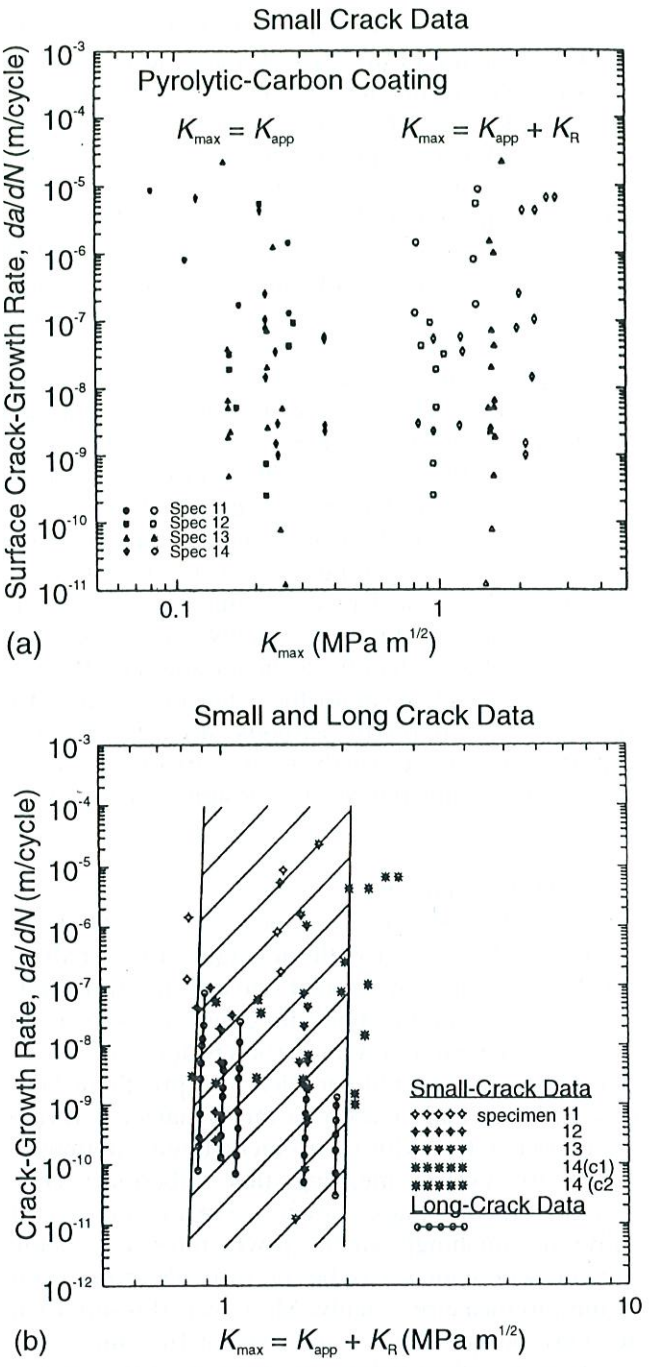

Figure 12: Experimental data showing cyclic fatigue-crack propagation rates, da/dN, in pyrolytic-carbon coated graphite for long through-thickness (edge) cracks and physically-small surface cracks, showing (a) small-crack data plotted as a function of K_{max}, computed from the externally applied loads ($K_{max} = K_{app}$; filled symbols) and in terms of contributions from both the applied loads and the residual stress field of the indent ($K_{max} = K_{app} + K_R$; open symbols); and (b) comparison of the growth rates of both long and small surface cracks as a function of $K_{max} = K_{app} + K_R$. Note the correspondence between long and small crack data where K_{max} incorporates both applied and residual stresses (37).

≈2 to 3 mm in length), pre-existing, through-thickness (edge) cracks (12,13,25,38,39). Although life prediction based on such data is perfectly standard for numerous applications in the aerospace and nuclear industries, for example, it has been increasingly recognized that a more complete analysis must include consideration of the apparently rapid growth of 'small' surface cracks, particularly in smaller component cross-sections such as those found in heart valve prostheses.

This is particularly important since it is well known for metal fatigue (53-55), and has recently become apparent for the fatigue of ceramics (42,56), that where cracks are physically small (typically below ≈500 μm), or small compared to microstructural dimensions or the extent of local crack-tip inelasticity, their growth rates can be far in excess of corresponding long cracks subjected to the same applied K levels; moreover, small cracks are known to propagate at applied stress intensities less than the fatigue threshold, below which long cracks are presumed to be dormant (42,53-56).

In valves with pyrolytic carbon components, analysis of in vivo failures has shown that small cracks can initiate at material defects, or from regions suffering cavitation erosion, in the pyrolytic-carbon coating (10); such cracks are typically semi-elliptical, part-through, surface cracks with dimensions less than a few hundred microns over the vast majority of the device life. Since most life-prediction analyses (12,13) currently use long-crack results (Fig. 8), it is important to show that these data adequately reflect the growth-rate properties of such small surface cracks.

Techniques for the measurement of small-crack growth rates are shown in Figure 4b and involve monitoring the top (polished) surface of cantilever-bend specimens cycled in 37°C Ringer's solution (26,37). Several Vicker's hardness indentations are placed along this surface; the residual tensile stress field surrounding the indent, together with half penny-shaped radial/median microcracks emanating from the indent corners (at $P_{int} > 9$ kg), act to facilitate fatigue-crack initiation (Fig. 5). Typically, an increasing bending stress range, $\Delta\sigma_b$ (≈10 to 80 MPa) is applied until one crack begins to grow, whereupon the stress is held constant until subsequent crack arrest; the procedure is then repeated. Tests are periodically interrupted every 10^2 to 10^4 cycles to permit the use of optical microscopy or gold-coated cellulose-acetate replicas to monitor crack growth. Full details are given in reference #37.

For the indentation crack configuration, there are two contributions to the stress intensity, namely that due to the applied stresses and that due to the residual stress field surrounding the indent, i.e., $K = K_{app} + K_R$. The stress-intensity factor resulting from the residual stress, K_R, can be calculated from the peak indentation load, P_{int}, and the half surface-crack length, c, using

Equations 4 and 5. Linear-elastic solutions for the applied K_{app} are given in reference #57 for three-dimensional semi-elliptical surface cracks in bending (and/or tension) in terms of the crack depth a, surface crack length $2c$, elliptical parametric angle ϕ, shape factor Q, specimen thickness t, specimen width b, and remote (outer surface) bending stress σ_b, from the applied load P_{app} (Fig. 4b):

$$K = H_c \sigma_b \left(\frac{\pi a}{Q}\right)^{1/2} F(a/c, a/t, c/b, \phi), \qquad (8)$$

where H_c is the bending multiplier and F is the boundary correction factor, the form and functional dependencies of which are detailed in reference #57. Equation 8 is valid for $0.2 \le a/c \le 1$ and $0° \le \phi \le 90°$ at $c/b \le 0.5$. It is worth noting that with increasing crack length, K_R decreases monotonically, independent of the applied loads, while K_{app} typically increases dependent upon the applied load levels; correspondingly, as the crack grows out of the field of the indent, the total K may show an initial reduction followed by a steady increase.

Typical results showing the crack-growth rate behavior, derived from the extension per cycle of the surface (trace) length of small cracks (≈100 to 500 μm) emanating from the indent corners in the pyrolytic-carbon coating, are plotted as a function of the externally applied ($K_{max} = K_{app}$) and total ($K_{max} = K_{app} + K_R$) stress intensities in Figure 12a. When characterized in terms of K_{app}, small-crack growth rates display seemingly anomalous behavior, namely, a negative dependency on stress intensity, and crack growth at K levels between 0.08 and 0.36 MPa√m, well below the (long-crack) threshold K_{TH} of ≈0.7 MPa√m.

Such behavior, which has been reported for many metallic and ceramic materials (26,37,41,42,53-55), in general results from a diminished role of crack-tip shielding with cracks of limited wake. Crack-tip shielding mechanisms act to affect crack advance by altering the local stress intensity actually experienced at the crack tip (58,59). Such mechanisms, which act principally in the crack wake, include transformation toughening in ceramics, crack bridging in composites, and crack closure during fatigue crack growth.

Whereas the applied stress intensity increases with crack extension in the usual manner (as K_{app} is a function of $P_{app}a^{1/2}$), the total stress intensity, which is actually experienced at the crack tip and hence drives the crack may have a different functional dependence on crack size as it is derived from the superposition of the applied stress intensity with that due to shielding. Here the shielding results from the residual tensile stresses around the indent, which diminish as the crack extends away (K_R is a function of $P_{int}a^{-3/2}$ from Equ. 4).

These dependencies on crack size are such that K_R is largest when the crack is smallest whereas the total (near-tip) stress intensity ($K_{max} = K_{app} + K_R$) may exhibit a minimum as the crack advances. Accordingly, when small-crack data are plotted in the usual way in terms of the externally applied loads, a negative dependency on stress intensity will be seen. However, when the full driving force is calculated taking into account the contributions from both applied and shielding (residual) stresses, the true positive dependency of growth rates on K_{max} is achieved (Fig. 12a).

From the perspective of prosthesis design, of prime importance here is that a close correspondence is achieved when the appropriately characterized small surface-crack data are compared with corresponding long edge-crack results, similar to those reported recently for SiC-whisker reinforced alumina (42). This normalization is shown for pyrolytic carbon in Figure 12b, although both forms of data are marked by extensive scatter. Moreover, at the same K_{max}, small-crack growth rates tend to be somewhat faster than corresponding long-crack rates. Although probably associated with scatter, this may result from an overestimation of K_R due to relaxation of the tensile residual stresses from the recovery of the pyrolytic carbon following removal of the indenter.

Thus, although current analyses use data on long through-thickness (edge) cracks whereas actual flaw growth in vivo is more likely to arise from small, semi-elliptical cracks which occur predominantly on the pyrolytic-carbon coating surface and propagate both along the surface and depth-wise toward the graphite core, it appears from Figure 12 that a reasonable correspondence can be obtained between long and small crack behavior; this can be achieved provided growth rates are characterized in terms of the appropriate K, incorporating both external (applied) and internal (residual) stresses. Such internal residual stresses may additionally result from fabrication processes, including coating deposition, machining and polishing, or be associated with surface damage such as scratches or gouges incurred during handling of the device. This is additionally important as the collection of such small-crack data in pyrolytic-carbon materials is both complex and extremely labor-intensive. Nevertheless, with appropriate characterization, in principle either form of growth-rate data may be used for design and life-prediction analyses.

Post-failure analysis (Fractography)

Examination of the fracture surface (fractography) of broken components can generally provide vital clues as to the cause of their failure. In metals, this follows because the morphology of fatigue fracture surfaces, which would have involved a long term progressive failure, are quite distinct from an impact or overload

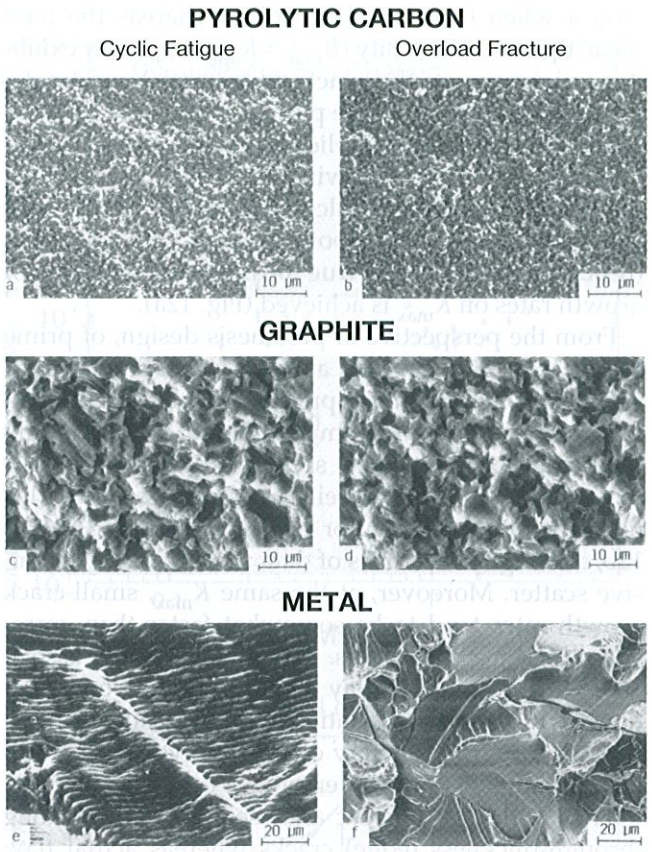

Figure 13: Scanning electron micrographs of cyclic fatigue and overload (fast) fracture in (a,b) the pyrolytic-carbon coating, (c,d) the polycrystalline graphite substrate, and (e,f) a metallic material (low-strength ferritic steel), showing (e) fatigue striations and (f) transgranular cleavage fracture (11).

fracture, which would have occurred in a single instance. Unfortunately, contrary to early reports in the literature (10), the morphologies of cyclic fatigue, stress-corrosion cracking and overload fractures in carbon materials are essentially indistinguishable (11,25). Indeed, this identical morphology of fatigue and overload fracture surfaces is not unique to pyrolytic carbon (Fig. 13a, b); similar behavior is shown by the graphite core of the composite material (Fig. 13c, d), and by most ceramic materials where cyclic fatigue fractures have been documented (41).

This is in marked contrast to metallic materials, where the characteristic cyclic fatigue fracture mode, i.e., striations (Fig. 13e), is quite different to the transgranular cleavage (Fig. 13f), microvoid coalescence, or intergranular fracture seen for failure under monotonic loads.

There is, however, a clear change in the laminate material between fractures in the pyrocarbon coating and the graphite substrate as the latter surfaces are considerably rougher. Fracture surfaces in both the substrate and coating appear to be covered in fine-scale facets, the dimensions of which approach that of the grains or 'growth features' in the microstructure.

The implication of these results is that post-failure analysis of failed pyrolytic-carbon valves can be quite deceptive. Unlike in metallic components, it is clearly not feasible to rely solely on fractography to conclude whether a specific failure was associated with a progressive time-dependent fracture or an instantaneous event. There are, however, exceptions. Discolored or abraded regions often indicate a pre-existing defect or one which has been in existence for some time and abraded by the continual opening and closing of the crack. Similarly, evidence of proteinaceous debris or granular tissue, e.g., fibrin, on a fracture surface is a clear indication of a crack that has existed, or has been growing, for an extended period of time.

Finally, in the pyrolytic carbon/graphite laminate material, the direction of crack growth can generally be deduced by noting whether delamination occurs at the pyrocarbon/graphite interface (Fig. 14) (37). In fact, an example of such interfacial delamination can be seen in the micrograph of the in vivo leaflet failure in Figure 2. Since the pyrolytic carbon has both higher stiffness and higher strength than the graphite, cracks will propagate normally through the interface when traversing from the pyrolytic carbon to the graphite (Fig. 14a). However, they will be deflected at, or just prior to, the interface when propagating from the graphite into the pyrolytic carbon (Fig. 14b). This fact can be extremely useful in evaluating crack-path trajectories, especially for the purpose of locating the origin of a fracture, during the post-failure analysis of broken valve components.

Damage-tolerant lifetime predictions

The damage-tolerant approach

The prime purpose of determining the toughness and crack-growth properties of pyrolytic carbon materials is to be able to derive a conservative estimate of the lifetime of a specific heart valve prosthesis under worst-case conditions. Fracture-mechanics based damage-tolerant analysis provides an ideal methodology for this purpose. Specifically, the life of a component is estimated in terms of the time, or number of loading cycles, to propagate the largest pre-existing crack to failure. Accordingly, to determine life, the relevant crack-growth relationship representing the most likely mechanism of subcritical cracking (Equations 6 and 7), is integrated between the limits of the initial (pre-existing) crack size, a_o, to the final (critical) crack size, a_c, at which final catastrophic failure of the component occurs. Using Equation 6a as the crack-growth relationship for cyclic fatigue, which is the most damaging cracking mecha-

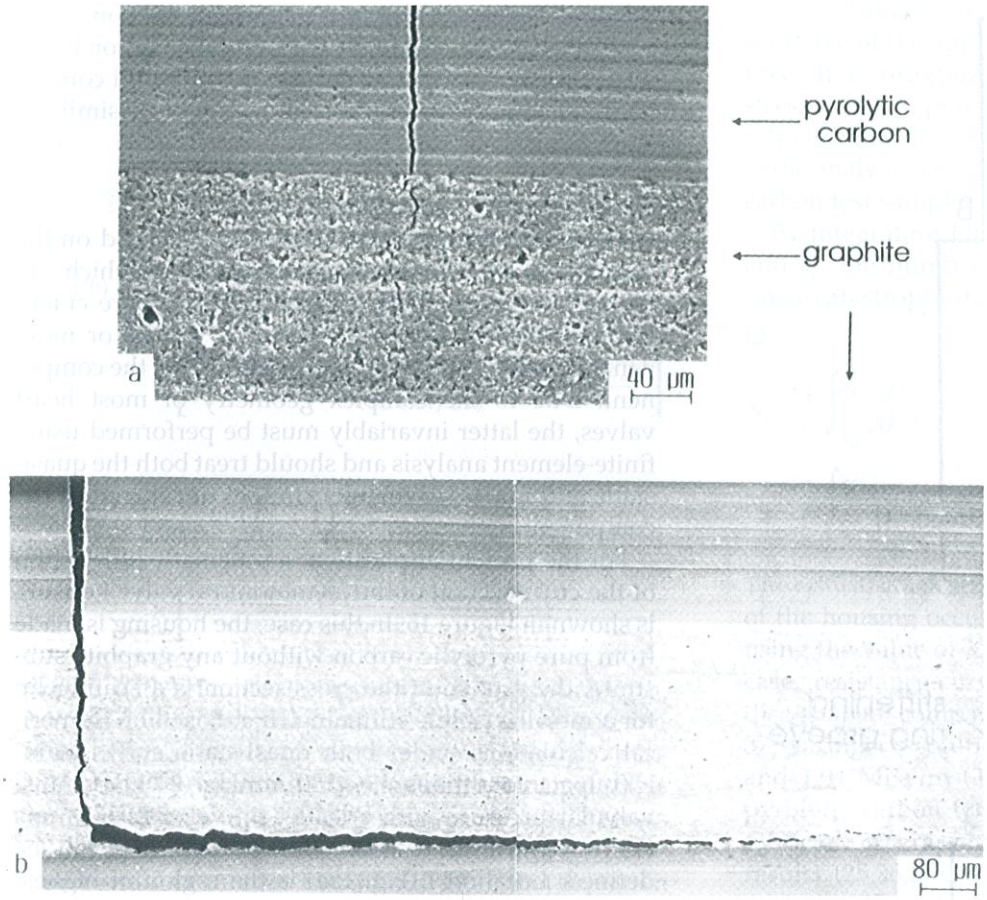

Figure 14: Scanning electron micrographs showing sections perpendicular to the crack plane for small-crack tests in pyrolytic-carbon coated graphite, showing (a) linear fatigue cracks propagating directly through the pyrocarbon-to-graphite (upper) interface, and (b) extensive crack deflection and delamination just prior to the graphite-to-pyrocarbon (lower) interface. The vertical arrow indicates the general direction of crack growth prior to deflection (26).

nism in pyrocarbons (25), with a K solution simply defined by Equation 1, the life of the component in terms of the number of loading cycles to failure can be written (for $m \neq 2$) as (12):

$$N_f = \frac{2}{(m-2)C(Q\Delta\sigma)^m \pi^{m/2}} [a_o^{-\{(m-2)/2\}} - a_c^{-\{(m-2)/2\}}] \quad (9)$$

where a_c can be computed from the critical crack size at final failure $K = K_c$, as shown in Equation 2.

Together with the level of applied stress, $\Delta\sigma$, and the crack-growth relationship, a critical input to this analysis is the initial crack size, which can be estimated by a number of different techniques. In aircraft components, for example, it can be defined by military standard, although a more appropriate procedure for medical implant devices is to evaluate a_o in terms of the largest undetected defect size; this initial crack size must be determined by non-destructive evaluation (NDE) procedures associated with the manufacturer's quality control before the device is implanted. NDE techniques such as imaging by optical and more importantly scanning electron microscopy have been used with success for metallic valves; however, as such microscopy only permits characterization of the surface of the device, a superior technique for pyrocarbon valves, where defects are as likely to be sub-surface, is to use a proof test which simulates the loading of the valve in vivo. Procedures for the design and use of such proof tests are discussed below.

Such damage-tolerant analyses are used regularly for many aerospace and nuclear components to evaluate safe lifetimes and moreover to dictate inspection intervals during service; typically, the first NDE inspection would be scheduled at half life, $^1/_2N_f$, to search for the presence of incipient cracks. Since for all practical purposes it is impossible to periodically examine cardiac devices once they are implanted, the damage-tolerant approach must be used somewhat differently, specifically to determine the pre-existing crack size that can never grow to failure within a patient lifetime, i.e., $\approx 10^9$ cycles or approximately 25 to 100 years or more. This minimum required detectable crack size then represents the defect size that must be detected by quality-control procedures prior to the device entering service in order to prevent mechanical failure of the prosthesis during patient lifetime. In metallic heart valves, the minimum detectable defect size is of the order of several hundreds of microns (12), which can be readily detectable with microscopy; for pyrocarbon valves, however, it is considerably smaller and can be of the order of several tens of microns for through-thickness edge cracks (13).

Application to heart valve prostheses

To illustrate how such procedures can be used for the design and safe operation of a prosthetic device, we will apply the damage-tolerant approach to an actual pyrolytic-carbon mechanical heart valve to estimate a conservative lifetime and hence the crack sizes that are

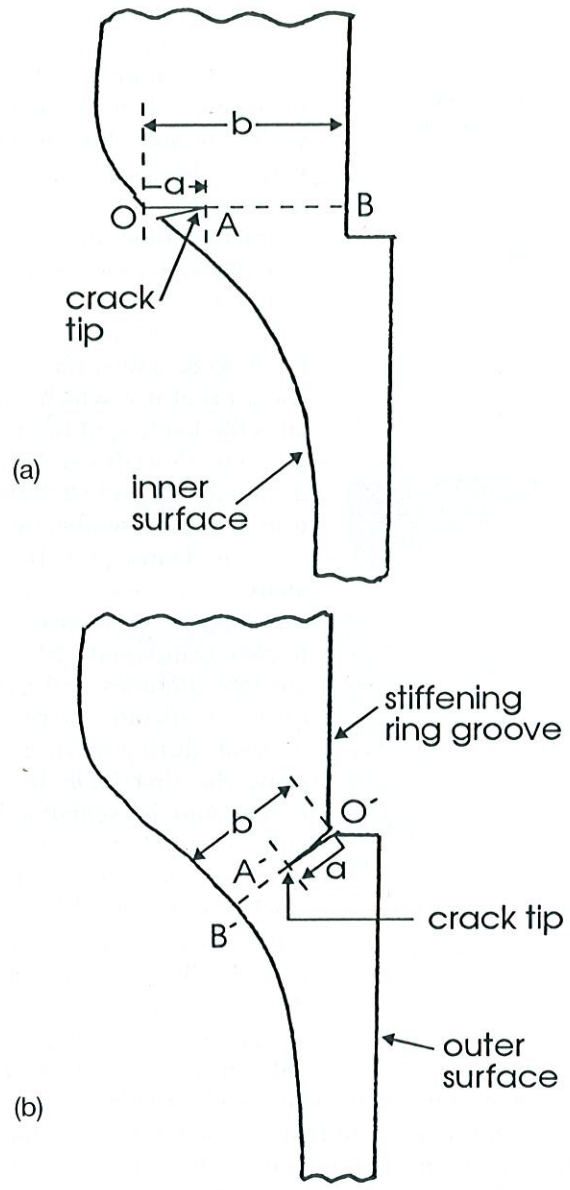

Figure 15: Schematic illustrations of the critical locations of cracks in the valve housing, showing (a) Location I - the highest (dynamic) stressed region on the inside of the seating lip, and (b) Location II - the highest stressed region on the outside surface of the housing at the upper corner of the stellite stiffening ring groove (13).

required to be detected by quality-control procedures to ensure adequate life. We will examine a valve of bileaflet design (Fig. 1) and, to preserve a worst-case scenario, consider the most highly stressed size, in this case the 29 mm mitral valve, with minimum in-tolerance dimensions and subjected to continuous elevated physiologic loading and environmental conditions. Moreover, worst-case assumptions will be additionally made with respect to cracking configurations, mechanical properties, and the pre-existence of defects in the material. For the purposes of this article, only one component of the valve, namely the pyrolytic-carbon housing, will be examined; in reality of course, all components including the leaflets, etc., would be similarly analyzed.

Stress and stress-intensity analyses

The life-prediction analysis must be focused on the critical and most highly stressed locations, which can be defined by practical experience, i.e., where cracks have formed on failed or explanted valves, or more generally on the basis of a stress analysis of the component. Due to the complex geometry of most heart valves, the latter invariably must be performed using finite-element analysis and should treat both the quasi-static and impact (dynamic) stresses developed in the component.

For the present application, a schematic illustration of the cross section of the 29 mm mitral valve housing is shown in Figure 15. In this case, the housing is made from pure pyrolytic carbon without any graphite substrate; the groove in the cross-section is a seating lip for a metallic stellite stiffening ring. Based on numerical calculations under both quasi-static and dynamic/impact conditions, i.e., 180 mmHg (24 kPa) transvalvular pressure with a leaflet tip velocity of 5 m/s (13), two critical locations for examination can be defined; Location I (Fig. 15a) is the region of highest (dynamic) stresses on the inside surface of the housing in the seating lip area, where the maximum surface stress is 5.5 MPa (calculated for quasi-static conditions) and 30.1 MPa (calculated for worst-case dynamic conditions), and Location II (Fig. 15b) is the highest stressed region on the outside surface of the housing at the upper corner of the stiffening ring groove, where the maximum surface stress is 43.3 MPa (calculated for dynamic conditions), assuming a corner root radius of 0.07 mm.

In addition to the externally applied stresses, residual stresses pre-existing in the housing must also be considered. Based on the hole-drilling tests (13) on pyrolytic-carbon coated graphite valve leaflets, the residual stresses were found to be approximately uniform within the coating with a value of $\sigma_R = 34 \pm 14$ MPa. Accordingly, for calculation purposes, a uniform residual stress of $\sigma_R = 48$ MPa is taken as a conservative estimate for the monolithic pyrolytic-carbon housing material.

For both critical locations on the housing, worst-case, through-thickness, edge cracks, which penetrate the free surface, are assumed to pre-exist and to follow a path dictated by the distribution of maximum tensile stress and minimum cross-sectional dimensions. An overestimate of the mode I stress-intensity factor for these cracking configurations is given by (13):

$$K = (\pi a)^{1/2}[F_m(a/b)S_m + F_b(a/b)S_b] \quad (10)$$

where

$$S_m = \sigma_o + {}^1/_2(\sigma_A - \sigma_o) \cdot (b/a) + \sigma_R \quad (10A)$$

$$S_b = \sigma_t - {}^1/_2(\sigma_A - \sigma_o) \cdot (b/a)$$

$$F_m(a/b) = \left(\frac{2b}{\pi a} \cdot \tan\left(\frac{\pi a}{2b}\right)\right)^{1/2} \times \left[\frac{0.752 + 2.02(a/b) + 0.37(1 - \sin(\pi a/2b))^3}{\cos(\pi a/2b)}\right]$$

$$F_b(a/b) = \left(\frac{2b}{\pi a} \cdot \tan\left(\frac{\pi a}{2b}\right)\right)^{1/2} \times \left[\frac{0.923 + 0.199(1 - \sin(\pi a/2b))^4}{\cos(\pi a/2b)}\right]$$

where, with reference to Figure 15, a is the crack length, b is the minimum cross-sectional width of the housing along the crack path, σ_o is the maximum tensile stress at the surface origin (i.e., the maximum principal stress in the orifice), and $\sigma_A(a)$ is the maximum tensile stress at the crack tip. The dimension b is 0.91 mm for Location I and 0.41 mm for Location II. Note that Equation 10 overestimates the stress intensity, especially at small crack sizes where $a/b \rightarrow 0$ (13). In addition, for the lifetime analyses described below, σ_R can be omitted as the residual stress pre-exists in both the mechanical property test specimens and the valve components.

Subcritical crack growth by cyclic fatigue

All existing cracks in the housing are assumed to propagate subcritically from the onset of loading in physiologic service; crack extension by cyclic fatigue is considered to occur with a loading frequency of 1.2 Hz (equivalent to 72 heart beats per minute or 38 x 10^6 cycles per year) with no incubation or crack initiation time. Based on cyclic fatigue experiments on pure pyrolytic carbon disc-shaped compact specimens tested in Ringer's solution at 37°C, the worst-case subcritical crack-growth rates can be described by the relationships (13,38):

$$da/dN = C(\Delta K)^m = 4.15 \times 10^{-3}(\Delta K)^{88.9} \quad [\text{units: m/cycle. (MPa}\sqrt{\text{m}})^{-m}]. \quad (11)$$

For the reasons described above, the existence of a threshold for no crack advance is discarded in the present analysis in order to be conservative; crack growth is thus permitted to occur at vanishingly small stress intensities, according to Equation 11. This relationship was determined for a load ratio of close to zero, representative of the applied "zero-tension" loading seen in vivo. It is recognized that the existence of residual stresses in the pyrolytic carbon will change this load ratio locally. However, this is not explicitly considered in the analysis since these stresses also exist in the pyrocarbon test samples.

By integrating Equation 11 between the limits of a_o and a_c, the number of loading cycles N_f required to cause catastrophic failure by cyclic fatigue is thus given by:

$$N_f = \frac{1}{C}\int_{a_o}^{a_f} \frac{da}{\Delta K^m} \quad (12)$$

$$N_f = \frac{1}{C}\int_{a_o}^{a_f} \frac{da}{[F_m(a/b)S_m + F_b(a/b)S_b]^m \pi^{m/2} a^{m/2}}.$$

The critical crack sizes, a_c, at which catastrophic failure of the housing occurs, are computed from Equation 2 using the value of K_c for pure pyrolytic carbon. In this case, resistance-curve results for fatigue-precracked, disc-shaped compact-tension samples, performed in 37°C Ringer's solution, yielded K_c values between 0.9 and 1.04 MPa$\sqrt{\text{m}}$ (38). (Note that K_c values for pure pyrolytic carbon tend to be lower than those for the pyrocarbon/graphite composite). In light of published results (25,26,37-39), an estimate of K_c = 1.0 MPa$\sqrt{\text{m}}$ was taken. It should be noted that because of the mathematical nature of the analysis, the precise value of K_c (in the range 0.8 to 2.5 MPa$\sqrt{\text{m}}$) has little effect on the numerical results.

Integration of Equation 12 using numerical proce-

Table II: Predicted lifetime for cyclic fatigue of the housing as a function of initial crack size, a_o, under worst-case physiological loading.

Initial Crack Size, a_o (μm)	Projected Cycles to Failure, N_f (cycles)	Lifetime (years)*
Location I:		
63	4.4×10^{10}	1.2×10^3
66	2.7×10^9	75.6
68	5.6×10^8	15.6
72	2.3×10^7	8 months
128	0	0
Location II:		
43	1.4×10^{11}	3.8×10^3
45	4.5×10^9	125
47	5.3×10^8	15
51	1.1×10^7	4 months
80	0	0

*assuming 38 x 10^6 cycles per year.

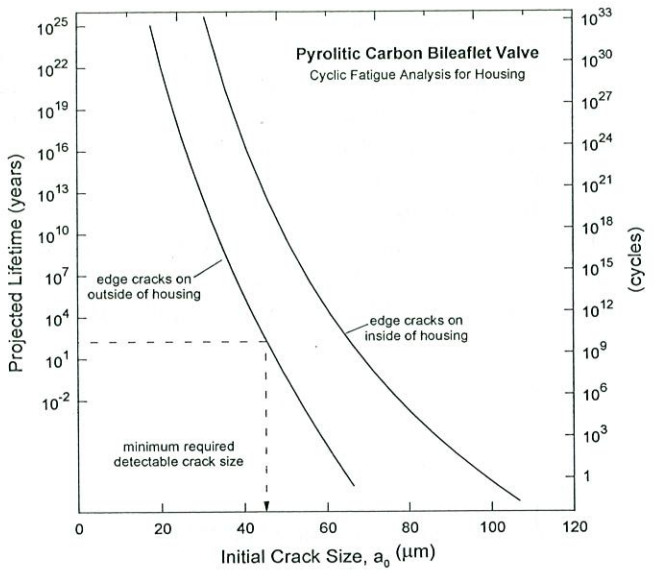

Figure 16: Damage-tolerant lifetime predictions of the minimum life of the valve housing as a function of the initial defect size, a_o, pre-existing in the component. Predictions pertain to worst-case through-thickness edge cracks in minimum dimension 29 mm mitral bileaflet valves, subjected to continuous peak physiologic loading conditions at Location I on the inside of the housing and Location II on the outside.

dures yields estimates of the number of cycles to failure, and hence life of the housing, under worst-case conditions as a function of the defect size a_o pre-existing in the housing. The resulting predictions are plotted schematically in Figure 16; specific numerical results for both cracking locations are listed in Table II. It is apparent that any pre-existing edge crack in the housing of a length in excess of $a_o \approx 66$ μm inside the orifice at the seating lip Location I and ≈45 μm outside the orifice at Location II can grow by cyclic fatigue and cause failure within 10^9 cycles, or within 100 years or so. The critical crack size at housing failure is between $a_c \approx 80$ and 128 μm depending upon the location.

Corresponding analyses for the leaflets on this valve yield detectable and critical edge crack sizes which are approximately a factor of two larger (13). Thus, provided NDE procedures can reliably detect all edge cracks in excess of a length of 45 μm in the housing prior to the valve entering service, the most conservative estimates of the damage-tolerant life in Table II imply that this component is capable of remaining operational under continuous peak in vivo loading for periods exceeding patient lifetimes.

Subcritical crack growth by stress-corrosion cracking

A similar worst-case analysis can be performed for subcritical crack-growth by stress-corrosion cracking. Based on sustained-load tests on pure pyrolytic carbon disc-shaped compact specimens tested in Ringer's solution at 37°C, the worst-case subcritical crack-growth rates are given by (13,38):

$$da/dt = C''(K)^n = 1.36 \times 10^{-7}(K)^{13.8} \quad [\text{units: m/sec. (MPa}\sqrt{\text{m}})^{-n}]. \quad (13)$$

Note again that the use of Equation 13 is conservative in that no crack-growth threshold is assumed; cracks can thus continue to grow at vanishingly small K levels.

As with cyclic fatigue, by integrating the crack-growth equation between the limits of initial to final crack size, the life of the housing L is given by the time t required for an edge crack to propagate from a_o and a_c:

$$L = t = \frac{1}{C''}\int_{a_o}^{a_f} \frac{da}{K^n} = \frac{1}{C''}\int_{a_o}^{a_f} \frac{da}{[F_m(a/b)S_m + F_b(a/b)S_b]^n \pi^{n/2} a^{n/2}}. \quad (14)$$

Results showing the life, L, as a function of the pre-existing defect size, a_o, based on numerical integration of Equation 14, are listed in Table III for edge cracks both inside (Location I) and outside (Location II) the housing. It is apparent that any pre-existing edge crack in the housing of a length in excess of $a_o \approx 82$ μm on the inside of the orifice (Location I) and ≈55 μm on the outside of the orifice (Location II) can potentially grow by stress corrosion and cause failure of the housing within 100 years or so. Since these estimates represent larger crack sizes than will cause failure by cyclic fatigue (Table II), the cyclic fatigue process is clearly rate limiting with respect to the service life of the housing such that the required minimum detectable crack size remains as 45 μm.

Table III: Predicted lifetime for the stress corrosion of the housing as a function of initial crack size, a_o, under worst-case physiological loading.

Initial Crack Size, a_o (μm)	Lifetime, L (years)
Location I:	
34	1.2×10^{30}
58	6.8×10^{11}
73	1.2×10^{5}
82	96
84	15
128	0
Location II:	
25	3.5×10^{24}
48	1.9×10^{6}
55	140
57	15
80	0

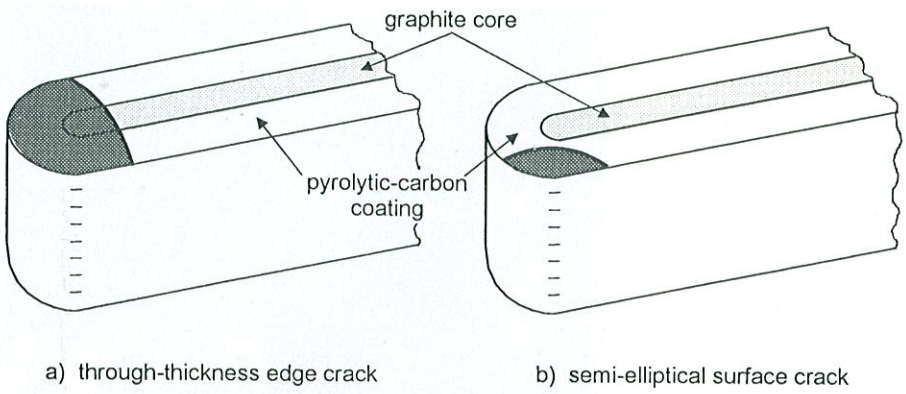

Figure 17: Schematic illustrations of (a) a through-thickness edge crack, and (b) a semi-elliptical surface crack in a pyrolytic-carbon coated graphite leaflet.

Consideration of semi-elliptical surface flaws

The damage-tolerant analyses described above are designed to be highly conservative; this is apparent with respect to the presumption of pre-existing defects in the valve component, the choice of minimum dimension valves, continuous elevated physiologic loading conditions, worst-case cracks in highest stressed locations, K solutions which overestimate the stress-intensity levels, worst-case subcritical crack-growth behavior induced at the immediate onset of loading in blood-analog environments (i.e., with no crack initiation period), and the assumption of the absence of a fatigue threshold for no crack growth.

The specific analysis performed in this study can be considered as the most conservative as it pertains to the extension of worst-case through-thickness edge cracks. Based on this analysis (and in practice that for the other components of the valve (13)), we have reasonably concluded that if final quality-control/NDE procedures can be designed to find, and correspondingly reject, all housings that contain defects exceeding 45 μm in size, the heart valve prosthesis should certainly survive in vivo long enough to ensure the safety of the patient.

From an engineering perspective, however, reliable detection of cracks as small as 50 μm in every valve is a difficult proposition, although to ensure the highest degree of safety, this is what is required. Moreover, many of the cracks seen on explanted and failed valves are not necessarily through-thickness edge cracks which extend across the whole section, but rather semi-elliptical cracks which penetrate from the free surface (Fig. 17). It is therefore appropriate additionally to consider the latter kind of defect as the value of K will invariably be lower than that for the corresponding edge crack of the same depth.

The stress-intensity solution for a semi-elliptical surface crack is given in Equation 8; although K values may vary around the crack front, calculations based on this equation yield initial and final crack sizes that are significantly larger than those computed above. For example, to ensure lifetimes in excess of 100 years in the present valve under peak in vivo stresses, the required detectable crack size for a semi-elliptical surface crack is approximately a factor of two larger in depth than that for the edge crack (13). Accordingly, from the perspective of designing quality-control procedures to screen new valve prostheses for the presence of defects, it is important to distinguish between the two types of cracks. For the bileaflet valve currently under consideration, this translates into developing quality-control procedures which can reliably find all edge cracks in the housing in excess of approximately 45 μm and all semi-elliptical surface cracks with depths in excess of approximately 100 μm. Techniques to accomplish this are described below.

Quality control: proof testing

The detection of cracks with dimensions in the tens of microns in small components such as heart valve prostheses poses real challenges for quality control. Although optical and scanning electron microscopy can be used successfully for metallic valves where required detectable crack sizes are several hundreds of microns in size (12), it would be difficult, if not impossible, to apply these techniques reliably to pyrocarbon valves because critical defect sizes are significantly smaller, crack-opening displacements are substantially reduced, and most importantly cracks in pyrolytic carbon are often sub-surface and thus invisible to optical and electron microscopy. Moreover, the defect sizes are essentially beyond the reliable detection range of other commercially available NDE techniques, such as ultrasonics and X-rays. In view of this, by far the best procedure for this application, in fact for many ceramic components, is through the use of the proof test.

The principle behind the proof test is to load each component to a pre-determined stress which is higher at each location than the stress that it would experience in service (60). Since the component will fail when K exceeds K_c, components which contain cracks larger than the critical crack size a_c, based on the applied proof stress σ_p, will not survive the test. Thus, if the component does not fracture during the proof test, the (initial) pre-existing crack size in that component cannot exceed a_c, e.g., from Equation 2:

$$a_o < a_c = \frac{1}{\pi}\left(\frac{K_c}{Q\sigma_p}\right)^2. \quad (15)$$

The importance of this is that through the use of Equations 9 and 15, a minimum fatigue lifetime can immediately be estimated for a valve that survives a particular magnitude of proof stress. Furthermore, by adjusting the proof stress such that a_o is less than, or equal to, the minimum required detectable crack size, survival of the proof test implies that the specific valve contains no cracks large enough to propagate to failure within a patient lifetime, i.e., that the prosthesis is mechanically safe.

In the author's opinion, the proof test is the only reliable method currently available with sufficient sensitivity to evaluate quantitatively and non-destructively the pre-existing defect population in newly manufactured pyrolytic-carbon prostheses. However, for the test to perform properly, certain conditions must be met. First, although the test should be simple to conduct as it must be performed on each and every valve, it is nevertheless absolutely essential that the loading during the proof test accurately simulates the direction and location of the stresses that the prosthesis will experience in vivo; if this proves to be difficult with a single proof test, two or more tests may need to be designed, for example, for both the housing and the leaflets.

An example of such a proof test that mimics the in vivo effect of transvalvular pressure on the leaflets in a bileaflet valve is to apply pressure pneumatically to the assembled valve to close the leaflets momentarily. Second, the magnitude of the proof stress must be high enough to 'find' crack sizes as small as the required detectable crack size, yet not too large that a large percentage of the valves are destroyed during the test. Moreover, appropriate proof stress levels should be determined for both edge and surface cracks. With most pyrolytic carbon valves, these two requirements can be generally met with proof stresses some five to ten times larger than in vivo stresses.

Third, in contrast to lifetime analyses, upper-bound values of the fracture toughness and lower-bound values of the geometry factors in the relevant K solutions must be used in Equations 9 and 15 for a worst-case estimate of a_o. Finally, it is critical that the prosthesis is not damaged by the proof test itself, for example, by a pre-existing crack extending subcritically and arresting without catastrophic failure of the valve. Although such an event is unlikely to be due to the highly brittle nature of pyrolytic carbon, it is nevertheless vital that some method of crack monitoring be employed during the proof test to ensure, at least qualitatively, that subcritical cracking does not occur; mounting an acoustic emission probe on the loading train of the proof test to detect stress waves from such cracking is one way to achieve this.

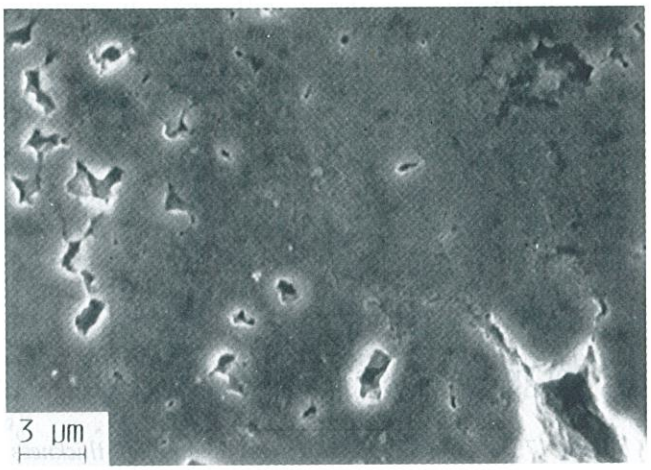

Figure 18: Scanning electron micrograph of the surface of the leaflet of an explanted pyrolytic carbon valve, showing evidence of small-scale pitting and the possible early stages of low level cavitation damage.

Concluding remarks

Careful mechanical design and life prediction, which must accurately simulate realistic failure modes, are essential elements for the reliable use of ceramic implants which will be exposed to complex physiologic loading and environmentally-induced degradation in clinical applications; in this regard, the structural design of cardiovascular-assist devices places particularly demanding requirements on the pyrolytic-carbon materials used as components of most heart valve prostheses. Specifically, to avoid patient trauma due to mechanical fracture of the valve, prostheses must be designed to endure fatigue lifetimes in excess of 10^9 cycles in simulated physiologic environments with failure rates probably no worse than one in 100,000.

The damage-tolerant procedures described in this article have been specifically developed to meet this need. They are designed to be highly conservative and thus are undoubtedly more costly than traditional design and life-estimation procedures that until recently have been common in this industry. However, in light of the individual tragedy of the potential loss of a life and the extremely high cost of litigation which will inevitably ensue, this is a small price to pay.

The approach is not without pitfalls, however. It should be remembered, for example, that the establishment of quality control and proof-test procedures to reliably reject all valves containing defects larger than the required detectable crack size will not necessarily assure safe lifetimes if cracks can develop subsequent to these NDE procedures. Should cracks, or even local-

ly roughened surfaces, be formed on the valve components due to inappropriate handling and implant procedures, during catheterization, or from cavitation damage in service (Fig. 18), lifetimes could be significantly shorter. It is therefore vital that procedures are established to minimize the possibility of such damage from occurring during handling or in vivo.

There is another factor to consider. Although pyrolytic carbon has been used successfully in hundreds of thousands of implanted valves and is clearly the current material of choice for this application, it is important to realize that from a purely engineering perspective, it is an extremely brittle material in the presence of cracks. In fact, to this author's knowledge, the pyrolytic-carbon heart valve is one of the few, if not the only, structural application where a ceramic-like material is used in a safety-critical situation, i.e., where material failure will most likely lead to loss of human life.

Furthermore, another inherent property of pyrolytic carbon and other ceramic-like materials is that subcritical crack-growth rates (at low homologous temperatures) are exceedingly sensitive to the stress-intensity level, i.e., the crack-growth exponents, m and n, in Equations 6 and 7 are invariably in the range of 10 to 100 or more (41). This means that the life of any pyrolytic-carbon component will be highly dependent upon the pre-existing defect size and the level of applied stress (specifically in damage-tolerant life-prediction procedures, life is proportional to σ^{-m} or σ^{-n}). As a result, small changes in a_o will lead to large changes in projected life, as can be seen in Tables II and III.

Moreover, since the crack-growth exponents can approach 100 in pyrolytic carbon, a factor of two increase in applied stress can result in a reduction in projected life by over 20 orders of magnitude! Since such sensitivity is an inherent feature of low toughness materials such as pyrolytic carbon, this alone is justification for design requirements with the highest degree of conservatism, as is afforded by the damage-tolerant approach.

Finally, it must be stated that the success of pyrolytic carbon as a material for prosthetic heart valves is undeniable; to date only a small number of components (probably less than about 50) in valves from several manufacturers are known to have failed after implant, and thereby to have produced life-threatening complications in patients. However, despite this record, it is still an undeniable fact that pyrolytic carbon is an inherently very brittle material and that mechanical failure in prosthetic devices is totally unacceptable, both socially and financially, particularly where loss of human life is involved. Accordingly, the use of worst-case damage-tolerant analyses must be regarded as an essential requirement for the design and quality control of new and existing 'ceramic' heart valve prostheses in order to provide maximum assurance of patient safety.

Acknowledgements

The author would particularly like to acknowledge Professor Reiner H. Dauskardt, now at Stanford University, Professor Robert M. McMeeking at UCSB and Dr. Avrom M. Brendzel at St. Jude Medical; much of the work described was performed in collaboration with them. Additionally, he would like to thank Dr. Jim McNaney for computational assistance, and Paul Schmidt and Ralph Kafesjian at Baxter, Ms. Diane MacCulloch, Dan J. Chwirut, and William F. Regnault at the FDA, Axel Haubold at the Medical Carbon Research Institute, Gene Stobbs at Medical Inc., Brett Demchuk at ATS Medical, and Al Beavan at Carbomedics for many useful discussions.

References

1. Bokros JC, Akins RJ, Shim HS, Haubold AD, Agarural NK. Carbon in prosthetic devices. In: Deviney MD, O'Grady TM (eds). Petroleum derived carbons. Washington D.C., American Chemical Society, 1976:237-265
2. Bokros JC. Carbon biomedical devices. Carbon 1977;15:355-371
3. Schoen FJ. Carbon in heart valve prostheses: foundation and clinical performance. In: Szycher M (ed). Biocompatible polymers, metals and composites. Lancaster, Technomic, 1983:239-261
4. Haubold AD, Yapp RA, Bokros JC. Carbons for biomedical applications. In: Bever MB (ed). Encyclopedia of materials science and engineering. Vol. 1. Oxford, UK, Pergamon Press/Cambridge, MIT Press, 1986:514-520
5. Dauskardt RH, Ritchie RO. Pyrolytic carbon coatings. In: Hench LL, Wilson J (eds). An introduction to bioceramics. Singapore, World Scientific Publ. Co., 1993:261-279
6. Larrieu AJ, Puglia E, Allen PA. Strut fracture and disc embolization of Björk-Shiley mitral valve prosthesis: localization of embolized disc computerized axial tomography. Ann Thorac Surg 1982;34:192-195
7. Lindblom D, Björk VO, Semb BKH. Mechanical failure of the Björk-Shiley valve: incidence, clinical presentation, and management. J Thorac Cardiovasc Surg 1986;92:894-907
8. Ostermeyer J, Horstkotte D, Bennet J. The Björk-Shiley 70° convexo-concave prosthesis strut fracture problem. Thorac Cardiovasc Surg 1987;35:71-77
9. Lindblom D, Rodriguez L, Björk VO. Mechanical failure of the Björk-Shiley valve. J Thorac Cardiovasc Surg 1989;97:95-97
10. Kelpetko V, Moritz A, Mlczoch J, H. Schurawitzki,

Domanig E, Wolner E. Leaflet fracture in Edwards-Duromedics bileaflet valves. J Thorac Cardiovasc Surg 1989;97:90-94

11. Ritchie RO, Dauskardt RH, Pennisi FJ. On the fractography of overload, stress corrosion and cyclic fatigue failures in pyrolytic-carbon materials used in prosthetic heart valve devices. J Biomed Mater Res 1992;26:69-76
12. Ritchie RO, Lubock P. Fatigue life estimation procedures for the endurance of a cardiac valve prosthesis: stress/life and damage-tolerant analyses. J Biomech Eng, Transactions of ASME 1986;108:153-160
13. Ritchie RO, McMeeking RM, Schmidt P, Lam HL. Damage-tolerant life-prediction procedures for the endurance of a pyrolytic-carbon mechanical heart valve prosthesis. J Biomed Mater Res 1996;30:(in press)
14. Chwirut DJ, Regnault WF. Fracture mechanics principles applied to implant medical devices-a review. Medical Progress through Technology 1988;14:193-203
15. Replacement Heart Valve Guidance Document. Washington, DC: Division of Cardiovascular, Respiratory, and Neurological Devices, Food and Drug Administration, U.S. Department of Health and Human Services, 1994
16. Kotlensky WV. Deformation in pyrolytic graphite. Trans Met Soc AIME 1965;223:830-832
17. Kotlensky WV, Martens HE. Structural changes accompanying deformation in pyrolytic graphite. J Am Ceram Soc 1965;48:135-138
18. Schoen FJ. On the fatigue behavior of pyrolytic carbon. Carbon 1973;11:413-414
19. Shim HS. The behavior of isotropic pyrolytic carbons under cyclic loading. Biomaterials and Medical Devices: Artificial Organs 1974;2:55-65
20. Kaae JL, Gulden TD, Liang S. Transmission electron microscopy of pyrolytic carbons deposited in a bed of fluidized particles. Carbon 1972;10:701-709
21. Bokros JC, LaGrange LD, Schoen FJ. Control of structure of carbon for use in bioengineering. In: Walker PL (ed). Chemistry and physics of carbon. New York, NY, Dekker, 1972:103-171
22. Kaae JL. Microstructures of pyrolytic carbon/silicon carbide mixtures co-deposited in a bed of fluidized particles. Carbon 1975;13:51-53
23. Pollmann E, Pelissier J, Yust CS, Kaae JL. Transmission electron microscopy of pyrocarbon coatings. Nuclear Technol 1977;35:301-309
24. Kaae JL. The effect of annealing on the microstructures and the mechanical properties of poorly crystalline isotropic pyrolytic carbons. Carbon 1972;10:691-699
25. Ritchie RO, Dauskardt RH, Yu W, Brendzel AM. Cyclic fatigue-crack propagation, stress-corrosion and fracture-toughness behavior in pyrolytic carbon-coated graphite for prosthetic heart valve applications. J Biomed Mater Res 1990;24:189-206
26. Ritchie RO, Dauskardt RH, Brendzel AM. Role of small cracks in the structural integrity of pyrolytic carbon heart valve prostheses. In: Ducheyne P, Christiansen D (eds). Bioceramics. Vol 6 (Proceedings of the 6th International Symposium on Ceramics in Medicine). Butterworths-Heinemann, 1993:229-236
27. Mitchell MR. Fundamentals of modern fatigue analysis for design. In: Fatigue and microstructure. Metals Park, OH, American Society for Metals, 1979:385-466
28. Annual book of ASTM standards. Vol. 3.01, Section 3.01. Philadelphia, PA, American Society for Testing and Materials, 1993
29. Tada H, Paris PC, Irwin GR. Stress analysis of cracks handbook. 2nd Ed. St. Louis, MO, Paris Publications/Del Research Corp., 1985
30. Lawn BR. Fracture of brittle solids. 2nd Ed. Cambridge, UK, Cambridge University Press, 1993
31. Lawn BR, Evans AG, Marshall DB. Elastic/plastic indentation damage in ceramics: the median/radial crack system. J Am Ceram Soc 1980;63:574-581
32. Ponton CB, Rawlings RD. Vickers indentation fracture toughness test. Part I. Review of literature and formulation of standardized indentation toughness equations. Mater Sci Tech 1989;5:865-872
33. Lawn BR, Fuller ER. Equilibrium penny-like cracks in indentation fracture. J Mater Sci 1975;10:2016-2024
34. Anstis GR, Chantikul P, Lawn BR, Marshall DB. A critical evaluation of indentation techniques for measuring fracture toughness: I. direct crack measurements. J Am Ceram Soc 1981;64:533-536
35. Ritchie RO, Francis B, Server WL. Evaluation of toughness in AISI 4340 alloy steel austenitized at low and high temperatures. Metall Trans A 1976;7A:831-838
36. More RB, Haubold AD, Beavan LA. Fracture toughness of Pyrolite^{R} carbon. Trans Soc Biomater 1989;15:180
37. Dauskardt RH, Ritchie RO, Takemoto JK, Brendzel AM. Cyclic fatigue and fracture in pyrolytic carbon-coated graphite mechanical heart valve prostheses: role of small cracks in life prediction. J Biomed Mater Res 1994;28:791-804
38. Ritchie RO, Dauskardt RH. Fracture toughness and subcritical crack-growth behavior of Pyrolite in simulated physiological environments. Technical report to CarboMedics, Inc., November 1990. Cited in: Beavan LA, James DW, Kepner J L. Evaluation of fatigue in Pyrolite^{R} carbon. In: Ducheyne P, Christiansen D (eds). Bioceramics. Vol 6. (Proceedings of the 6th International Symposium on Ceramics in Medicine). Butterworths-Heinemann, 1993:205-210
39. Gilpin CB, Haubold AD, Ely JL. Fatigue crack growth

and fracture of pyrolytic carbon composites. In: Ducheyne P, Christiansen D (eds). Bioceramics. Vol 6. (Proceedings of the 6th International Symposium on Ceramics in Medicine). Butterworths-Heinemann, 1993:217-223

40. Johnson HH, Paris PC. Sub-critical flaw growth. Eng Fract Mech 1968;1:3-45
41. Ritchie RO, Dauskardt RH. Cyclic fatigue in ceramics: a fracture mechanics approach to subcritical crack growth and life prediction. J Ceram Soc Japan 1991;99:1047-1062
42. Dauskardt RH, James MR, Porter JR, Ritchie RO. Cyclic fatigue-crack growth in SiC-whisker-reinforced alumina ceramic composite: long and small-crack behavior. J Am Ceram Soc 1992;75:759-771
43. Gilbert CJ, Dauskardt RH, Ritchie RO. Behavior of cyclic fatigue cracks in monolithic silicon nitride. J Am Ceram Soc 1995;78:2291-2300
44. Dauskardt RH, Ritchie RO. Cyclic fatigue-crack growth behavior in ceramics. Closed Loop 1989;17:7-17
45. Sines G, Ma Ling. Long life fatigue of pyrolytic carbon. In: Ducheyne P, Christiansen D (eds). Bioceramics. Vol 6. (Proceedings of the 6th International Symposium on Ceramics in Medicine). Butterworths-Heinemann, 1993:211-215
46. Beavan LA, James DW, Kepner JL. Evaluation of fatigue in Pyrolite^{R} carbon. In: Ducheyne P, Christiansen D (eds). Bioceramics. Vol 6. (Proceedings of the 6th International Symposium on Ceramics in Medicine). Butterworths-Heinemann, 1993:205-210
47. Ritchie RO. Near-threshold fatigue crack propagation in steels. Int Metals Rev 1979;20:205-230
48. Evans AG. Fatigue in ceramics. Inl J Fract 1980;16:485-495
49. Minnear WP, Hollenbeck TM, Bradt RC, Walker PL. Sub-critical crack growth of glassy carbon in water. J Non-Cryst Solids 1976;21:107-115
50. Soltesz U, Ritter H. Mechanical behavior of selected ceramics. In: Ducheyne P, Hastings GW (eds). Metals and ceramics biomaterials. Vol 2. Strength and surface. Boca Raton, CRC Press, 1984:23-61
51. Hodkinson PH, Nadeau JS. Slow crack growth in graphite. J Mater Sci 1975;10:846-856
52. Ely JL, Haubold AD. Static fatigue and stress corrosion in pyrolytic carbon. In: Ducheyne P, Christiansen D (eds). Bioceramics. Vol 6. (Proceedings of the 6th International Symposium on Ceramics in Medicine). Butterworths-Heinemann, 1993:199-204
53. Suresh S, Ritchie RO. The propagation of short fatigue cracks. Int Metals Rev 1984;29:445-476
54. Ritchie RO, Lankford J (eds.). Small fatigue cracks. Warrendale, PA, The Metallurgical Society of AIME, 1986:665
55. Miller KJ, de los Rios ER (eds.). The behaviour of short fatigue cracks. London, UK, Institute Mechanical Engineers, 1986:560
56. Steffen AA, Dauskardt RH, Ritchie RO. Cyclic fatigue life and crack-growth behavior of microstructurally-small cracks in Mg-PSZ ceramics. J Am Ceram Soc 1991;74:1259-1268
57. Raju IS, Atluri SN, Newman, JC Jr. Stress-intensity factors for small surface and corner cracks in plates. In: Wei RP, Gangloff RP (eds). Fracture mechanics: perspectives and directions (20th Symp.). ASTM STP 1020. Philadelphia, PA, Am Soc Testing Mater, 1989:297-316
58. Ritchie RO. Mechanisms of fatigue crack propagation in metals, composites and ceramics: role of crack-tip shielding. Mater Sci Eng 1988;103A:15-28
59. Evans AG. The new high toughness ceramics. In: Wei RP, Gangloff RP (eds). Fracture mechanics: perspectives and directions (20th Symp.) ASTM STP 1020. Philadelphia, PA, Am Soc Testing Mater, 1989:267-291
60. Evans AG, Wiederhorn SM. Proof testing of ceramic materials - an analytical basis for failure prediction. Int J Fract 1974;10:379-392